



# DDX3X and specific initiation factors modulate *FMR1* repeat-associated non-AUG-initiated translation

Alexander E Linsalata<sup>1,2</sup>, Fang He<sup>2,3</sup>, Ahmed M Malik<sup>2,4</sup> , Mary Rebecca Glineburg<sup>2</sup>, Katelyn M Green<sup>1,2</sup>, Sam Natla<sup>2</sup>, Brittany N Flores<sup>1,2</sup>, Amy Krans<sup>2</sup>, Hilary C Archbold<sup>2</sup>, Stephen J Fedak<sup>2</sup>, Sami J Barmada<sup>2</sup> & Peter K Todd<sup>2,5,\*</sup> 

## Abstract

A CGG trinucleotide repeat expansion in the 5' UTR of *FMR1* causes the neurodegenerative disorder Fragile X-associated tremor/ataxia syndrome (FXTAS). This repeat supports a non-canonical mode of protein synthesis known as repeat-associated, non-AUG (RAN) translation. The mechanism underlying RAN translation at CGG repeats remains unclear. To identify modifiers of RAN translation and potential therapeutic targets, we performed a candidate-based screen of eukaryotic initiation factors and RNA helicases in cell-based assays and a *Drosophila melanogaster* model of FXTAS. We identified multiple modifiers of toxicity and RAN translation from an expanded CGG repeat in the context of the *FMR1* 5'UTR. These include the DEAD-box RNA helicase *belle/DDX3X*, the helicase accessory factors *EIF4B/4H*, and the start codon selectivity factors *EIF1* and *EIF5*. Disrupting *belle/DDX3X* selectively inhibited *FMR1* RAN translation in *Drosophila in vivo* and cultured human cells, and mitigated repeat-induced toxicity in *Drosophila* and primary rodent neurons. These findings implicate RNA secondary structure and start codon fidelity as critical elements mediating *FMR1* RAN translation and identify potential targets for treating repeat-associated neurodegeneration.

**Keywords** DDX3X; eIF; Fragile X-associated tremor/ataxia syndrome; RAN translation; RNA helicase

**Subject Categories** Neuroscience; Protein Biosynthesis & Quality Control; RNA Biology

**DOI** 10.15252/embr.201847498 | Received 29 November 2018 | Revised 19 June 2019 | Accepted 26 June 2019 | Published online 25 July 2019

**EMBO Reports (2019) 20: e47498**

## Introduction

Over 30 different nucleotide repeat expansions (NREs) cause neurodegeneration in humans [1]. NREs within consensus coding sequences (CCDS) cause disease predominantly via protein-based

gain-of-function mechanisms that depend on the intrinsic toxicity of homopolymeric peptides or dysfunction of the proteins in which they reside [2–5]. Alternatively, NREs can elicit toxicity via mRNA-based mechanisms where expanded repeats sequester essential RNA-binding proteins, leading to transcriptome dysregulation (e.g., myotonic dystrophy I and II) and gelation of RNA-protein complexes into RNA containing foci [6–9]. More recently, NREs were found to support translational initiation in the absence of an AUG start codon through a process known as repeat-associated, non-AUG (RAN) translation [10]. Proteins generated through RAN translation accumulate in patient tissues [10–15] and are toxic in animal and cellular models of disease [10,14,16–18]. Since its discovery, RAN translation has been implicated in several NRE-associated neurodegenerative disorders [19], including Fragile X-associated tremor/ataxia syndrome (FXTAS), *C9orf72*-associated amyotrophic lateral sclerosis and frontotemporal dementia (C9ALS/FTD), and Huntington's disease [20].

FXTAS is an adult-onset neurodegenerative disorder caused by a CGG NRE in the 5' UTR of *FMR1* from approximately 30 repeats to 55–200 repeats [21]. The NRE is transcribed into mRNA, which can bind to and sequester specific RNA-binding proteins [22–27]. In addition, expanded CGG repeats are translated via RAN translation into toxic proteins, which accumulate in ubiquitinated aggregates in tissue of both FXTAS patients and animal models of FXTAS [14,17,18]. Synthesis of RAN products is necessary for CGG repeats to elicit toxicity in over-expression systems, including *Drosophila melanogaster*, cultured human cells, and transgenic mice [14,17,28]. FXTAS shares its causative locus with the neurodevelopmental disorder Fragile X syndrome, but it is clinically and mechanistically distinct: Fragile X syndrome results from larger (> 200) CGG NREs that transcriptionally silence the Fragile X locus, resulting in loss of *FMR1* mRNA, no expression of expanded CGG repeats as RNA, and loss of FMRP [29].

The mechanism of RAN translation, and how it differs from canonical translation, remains unclear. Early reports demonstrated that, at least under some circumstances, RAN translation's initial

1 Cellular and Molecular Biology Graduate Program, University of Michigan, Ann Arbor, MI, USA

2 Department of Neurology, University of Michigan, Ann Arbor, MI, USA

3 Department of Biological and Health Sciences, Texas A&M University, Kingsville, TX, USA

4 Neuroscience Graduate Program, University of Michigan, Ann Arbor, MI, USA

5 Ann Arbor VA Medical Center, Ann Arbor, MI, USA

\*Corresponding author. Tel: +1 734 615 5632; E-mail: petertod@med.umich.edu

†This article has been contributed to by US Government employees and their work is in the public domain in the USA

stages resemble canonical translation [30–32]: The 43S pre-initiation complex (PIC)—composed of the 40S ribosomal subunit, tRNAi<sup>Met</sup>, and a number of essential eukaryotic initiation factors (eIFs)—binds to the 5′ methyl-7-guanosine (m<sup>7</sup>G) cap on mRNA and scans through the 5′ untranslated region (UTR) [33]. In canonical translation, the 43S PIC scans until it encounters an AUG start codon, which triggers a cascade of structural rearrangements that ends with binding of the 60S ribosomal subunit and initiation of translation. In RAN translation, initiation occurs at non-AUG codons, either upstream of or within the NRE [10,30–32,34]. At CGG repeats and possibly GGGGCC repeats, this failure of codon fidelity is thought to result from impairment of 43S PIC scanning by stable RNA secondary structures formed by the expanded repeats, since such structures facilitate initiation at non-AUG sites [35–38]. At other repeats and cellular contexts, RAN translation may utilize cap-independent initiation mechanisms and/or initiator tRNAs other than tRNAi<sup>Met</sup> [10,39,40]. Which mechanisms occur in the context of each human disease is unclear and could vary based on gene context, repeat content, and cell type [19,41,42].

Discerning how RAN translation initiates, and how that process diverges from canonical translation, might reveal new therapeutic strategies for FXTAS, C9ALS/FTD, and other NRE-associated disorders. Two features distinguish RAN translation from canonical translation: the presence of highly stable RNA secondary structures composed of NREs [43–45] and the use of non-AUG start codons. 43S PIC scanning is known to require several RNA helicases in order to resolve mRNA structure within 5′ UTRs, including Ded1/Belle/DDX3X [46–52], eIF4A and its cofactors eIF4B and eIF4H [50,53–55], and DHX29 [56,57]. In addition, start codon fidelity in yeast is regulated by a series of eIFs—including eIF1, eIF1A, eIF2, and eIF5—and upstream signaling pathways [58–65].

With these features in mind, we conducted a candidate-based screen of eIFs, RNA helicases, and other RNA-binding proteins to identify regulators of RAN translation, using both cell-based assays and a *Drosophila melanogaster* model of FXTAS [66]. In FXTAS, RAN translation from the sense strand of *FMR1* yields at least two RAN products from the CGG repeat: a polyglycine peptide (FMRpolyG), reflecting initiation in the GGC (+1, relative to the reading frame of the downstream CCDS product, FMRP) frame, and a polyalanine peptide (FMRpolyA), reflecting initiation in the GCG (+2) frame [14,31]. Antisense *FMR1* transcripts also support RAN translation, yielding three distinct RAN products [67]. In *Drosophila*, we previously demonstrated that CGG repeat-associated toxicity is largely dependent on RAN translation [14,68]. Our screen identified multiple factors that were necessary for RAN translation from the *FMR1* 5′ UTR, disruption of which suppressed CGG repeat-associated toxicity in *Drosophila*. Disruption of one in particular, the DEAD-box RNA helicase *DDX3X* (*belle* in *Drosophila*), selectively inhibited *FMR1* RAN translation in human cell-based systems and suppressed repeat-induced neurodegeneration in rodent neurons. Our findings implicate RNA secondary structure and start codon fidelity in *FMR1* RAN translation and suggest specific targets for future therapeutic development.

## Results

### A *Drosophila* screen for modifiers of CGG repeat toxicity

To identify regulators of *FMR1* RAN translation, we conducted a candidate-based screen using a *Drosophila melanogaster* model of FXTAS

[66]. This model carries an EGFP transgene 3′ to an upstream activation sequence (UAS) and the 5′ UTR of human *FMR1* with 90 CGG repeats, with EGFP in the GGC (+1, FMRpolyG) reading frame [(CGG)<sub>90</sub>-EGFP]. The expression in the eye via a GMR-GAL4 driver manifests in a significant rough-eye phenotype observable at eclosion, with ubiquitin-positive aggregates of the RAN product FMRpolyG-EGFP accumulating in retinal neurons [14]. For the screen, females expressing (CGG)<sub>90</sub>-EGFP under a GMR-GAL4 driver were crossed to males carrying germline mutations in, UAS-driven transgenes of, and UAS-driven shRNA constructs to 10 canonical eIFs, 4 RNA helicases, a ribosomal protein associated with non-canonical translation initiation [69,70], and an RNA-binding protein implicated in ALS/FTD [71] (Appendix Fig S1). We selected these candidates in a hypothesis-driven fashion based on their known functions in non-canonical translation initiation and regulation of start codon fidelity, as well their potential to modulate GC-rich secondary structures in RNA. By design, this candidate list was non-exhaustive. Because previous work has demonstrated the importance of eIF4E-m<sup>7</sup>G binding and 43S PIC scanning to RAN translation [30–32] and because eIF4E and eIF4G are necessary for canonical translation, we did not evaluate them in this screen.

We examined the rough-eye phenotype of the F<sub>1</sub> flies at eclosion to identify suppressors and enhancers of (CGG)<sub>90</sub>-driven toxicity. Of the 57 candidate lines tested, 21 acted as suppressors of toxicity, and 17 acted as enhancers (Fig 1, Appendix Fig S1). All lines were subsequently crossed to flies carrying GMR-GAL4 alone to control for toxic effects independent of (CGG)<sub>90</sub>-based toxicity (Appendix Fig S1). Six of the 17 toxicity-enhancing lines had no effect in the absence of (CGG)<sub>90</sub>-EGFP, suggesting this enhancement is specific to the presence of expanded CGG repeats. We selected three suppressors for further analysis—*belle* (*bel*)/*DDX3X*, *eIF4B*, and *eIF4H1*—based on their individual functions in translation initiation.

### *Bel/DDX3X* selectively modulates *FMR1* RAN translation in *Drosophila*

In our candidate-based *Drosophila* screen, *bel* disruption by multiple genetic means suppressed CGG<sub>100</sub>-elicited toxicity. Four shRNAs against *bel* and five heterozygous loss-of-function *bel* mutants significantly suppressed the rough-eye phenotype in (CGG)<sub>90</sub>-EGFP-coexpressing flies (Fig 2A and B; Appendix Fig S2A and B). *Bel* mutants tested included nonsense mutations and P[lacW] and P[PZ] element insertions [72–75]. The *bel* shRNA lines generally suppressed (CGG)<sub>90</sub>-EGFP toxicity more effectively than the heterozygous, loss-of-function *bel* mutants, potentially because the shRNAs had stronger effects on the abundance of *bel* protein. None of the *bel* shRNAs had phenotypic effects in flies expressing an AUG-initiated EGFP transgene under a GMR-GAL4 driver (Appendix Fig S2C and D). Modulation of (CGG)<sub>90</sub>-driven toxicity was not limited to the eye, since three *bel* shRNAs increased the lifespan of adult flies expressing (CGG)<sub>90</sub>-EGFP ubiquitously post-eclosion under an inducible Tub5 Geneswitch driver (Fig 2C) [76]. Similarly, four *bel* shRNAs increased lifespan when (CGG)<sub>90</sub>-EGFP was expressed pan-neuronally in adult flies under an inducible Geneswitch ElaV driver (Fig 2D).

*Bel* and its homologs in yeast (*Ded1*) and humans (*DDX3X*) are important for translation of specific mRNAs, particularly those with long or structured 5′ UTRs [46–52,77]. Given the role that secondary structure is hypothesized to play in the initiation of RAN translation, we asked whether knockdown of *bel* suppressed the (CGG)<sub>90</sub>-EGFP

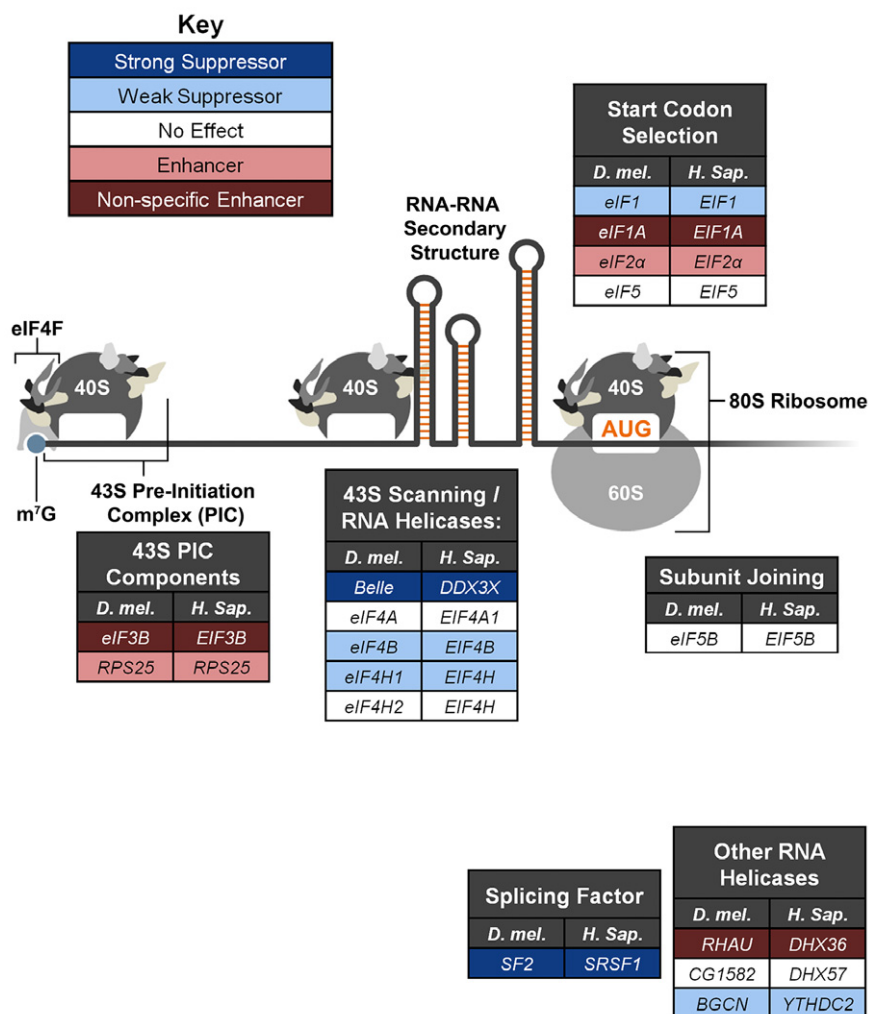


**Figure 1. A candidate-based screen reveals modifiers of repeat-associated toxicity in *Drosophila*.**

Candidate modifiers are categorized here based on their known functions in gene expression. Fly genes are listed in the left columns, while their human homologs are listed in the right columns. Disruption of genes highlighted in dark blue strongly suppressed (CGG)<sub>90</sub>-EGFP toxicity. Disruption of genes highlighted in light blue weakly suppressed (CGG)<sub>90</sub>-EGFP toxicity. Disruption of genes highlighted in light red enhanced (CGG)<sub>90</sub>-EGFP toxicity selectively. Disruption of genes highlighted in dark red enhanced the toxicity of both (CGG)<sub>90</sub>-EGFP and GMR-GAL4 (these were toxic independent of the repeat). All other genes are displayed in white. The methyl-7-guanosine (m<sup>7</sup>G) cap, eIF4F complex, 43S pre-initiation complex (PIC), and ribosomes are indicated.

phenotype by suppressing RAN translation. Knockdown of *bel* by two independent shRNAs reduced the expression of the RAN product FMRpolyG-EGFP in (CGG)<sub>90</sub>-expressing flies (Fig 2E and F), supporting the hypothesis that suppression of (CGG)<sub>90</sub> toxicity is driven by inhibition of RAN translation. In contrast, *bel* knockdown had no effect on the abundance of (CGG)<sub>90</sub>-EGFP transcripts (Fig 2G). Finally, knockdown of *bel* had no effect on the expression of an AUG-initiated EGFP reporter lacking the *FMR1* 5' UTR (Fig 2H and I), suggesting that the decrease in FMRpolyG-EGFP we observed reflects a selective effect on RAN translation, rather than a global decline in translation.

#### ***Bel/DDX3X* selectively modulates *FMR1* RAN translation in human cells**

We next asked whether *DDX3X*, the human homolog of *bel*, might play a similar role in facilitating RAN translation of CGG repeats in

human cells. We previously generated transfectable luciferase-based reporters consisting of a 3xFLAG-tagged nanoluciferase (NL-3xF) downstream of the 5'UTR of human *FMR1*, with multiple repeat sizes (0–100 repeats) and with the NL-3xF in both the GGC (+1, FMRpolyG) and GCG (+2, FMRpolyA) reading frames (Appendix Fig S3) [31]. These reporters enable quantitative and qualitative detection of RAN product expression by luminescence assays and Western blotting, respectively. Knockdown of *DDX3X* by five independent siRNAs reduced the expression of plasmid-based +1 (CGG)<sub>100</sub> NL-3xF reporters in a dose-dependent manner (Fig 3A; Appendix Fig S4). As in our *Drosophila* experiments, these siRNAs had minimal effect on the expression of an AUG-initiated NL-3xF reporter (AUG-NL-3xF). To further test whether *DDX3X* knockdown inhibits protein synthesis across mRNAs, we tested the effects of two *DDX3X* siRNAs on NL-3xF reporters bearing the short, minimally structured 5' UTRs of  *$\beta$ -actin* and  *$\beta$ -globin*. siDDX3X #1 had

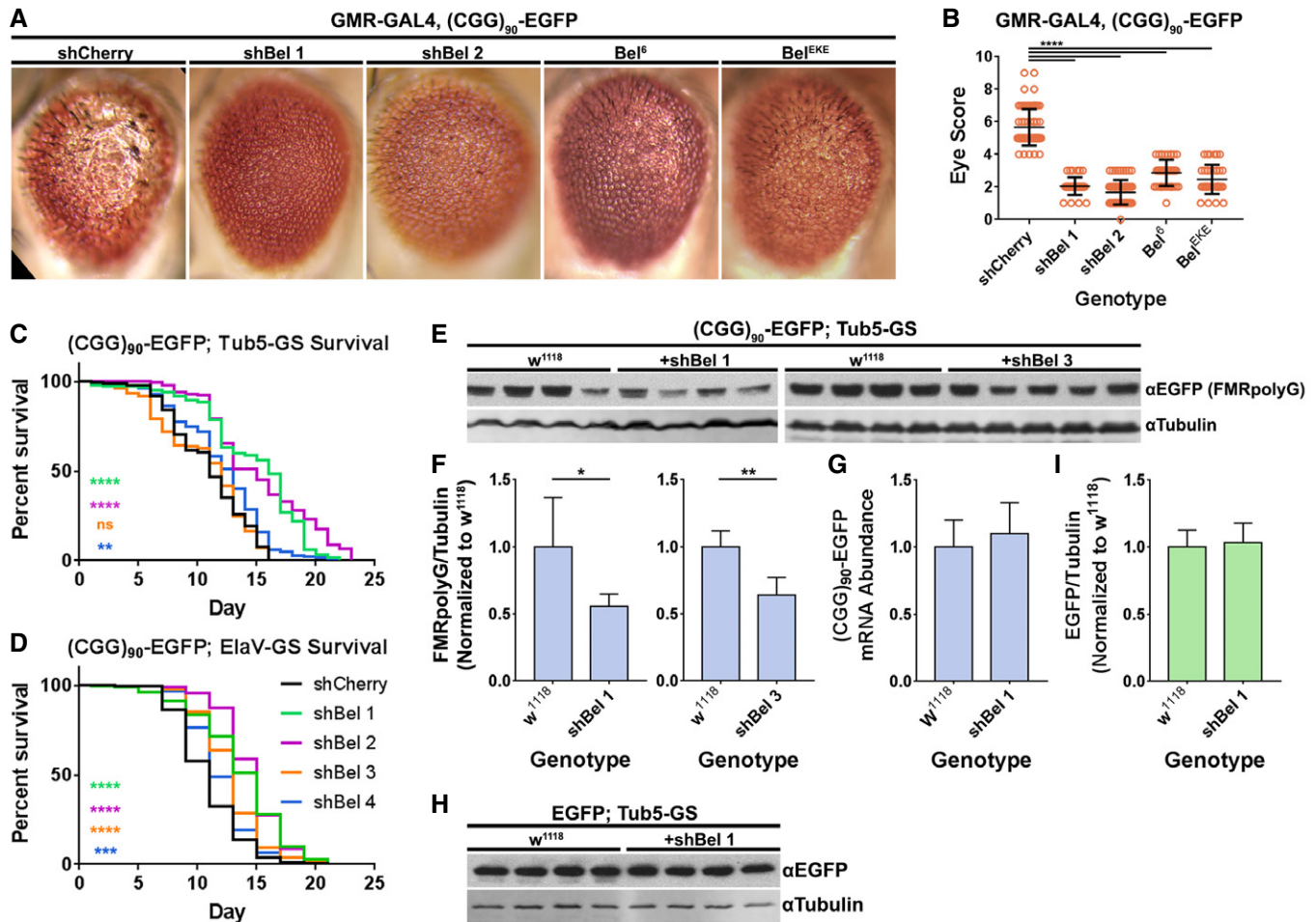


**Figure 2. Knockdown of *belle* mitigates repeat-associated toxicity by inhibiting RAN translation in *Drosophila*.**

- A Representative photographs of fly eyes expressing (CGG)<sub>90</sub>-EGFP under a GMR-GAL4 driver, with various *belle* disruptions.
- B Quantitation of GMR-GAL4 and (CGG)<sub>90</sub>-EGFP eye phenotypes with *belle* disruptions (Mann–Whitney *U*-test with Bonferroni corrections for multiple comparisons; *n* = 35–77/genotype).
- C, D Longevity assays of (CGG)<sub>90</sub>-EGFP; Tub5-GS (log-rank Mantel–Cox test with Bonferroni corrections for multiple comparisons; *n* = 110–219/genotype) and (CGG)<sub>90</sub>-EGFP; ElaV-GS (*n* = 147–299/genotype) flies with *belle* knockdown.
- E Western blots of the FMRpolyG-EGFP RAN product in (CGG)<sub>90</sub>-EGFP; Tub5-GS flies with and without *belle* knockdown by two independent shRNAs.
- F Quantitation of FMRpolyG-EGFP band density, normalized to β-tubulin band density, from blots in (E) (Student's *t*-test; *n* = 4–5/genotype).
- G Abundance of (CGG)<sub>90</sub>-EGFP mRNA normalized to *RPL32* mRNA, following *belle* knockdown, determined by qRT-PCR (*n* = 8/genotype).
- H Western blot of AUG-driven EGFP in EGFP; Tub5-GS flies with and without *belle* knockdown.
- I Quantitation of EGFP band density, normalized to β-tubulin band density, from blot in (H) (*n* = 4/genotype).

Data information: For all panels, \**P* ≤ 0.05, \*\**P* ≤ 0.01, \*\*\**P* ≤ 0.001, \*\*\*\**P* ≤ 0.0001 for the specified statistical test. All data in all panels are presented as mean ± SD (compiled from ≥ 3 replicates).

no effect on Actin-NL-3xF and increased the expression of Globin-NL-3xF but decreased the expression of +1 (CGG)<sub>100</sub> NL-3xF (Appendix Fig S5A). Though siDDX3X #2 decreased both Actin- and Globin-NL-3xF, it did so significantly less than it inhibited +1 (CGG)<sub>100</sub> NL-3xF. Finally, to assess the effects of *DDX3X* knockdown on global protein synthesis of endogenous mRNAs, we performed polysome fractionation on HeLa cells transfected with siDDX3X or siEGFP (Appendix Fig S6A and B). Consistent with our NL-3xF reporter data, knockdown of *DDX3X* (Appendix Fig S6C) did not result in a reproducible shift in the relative monosome and polysome fractions. This indicates that *DDX3X* knockdown does not lead to global inhibition of mRNA translation, again highlighting the role

of *DDX3X* in the expression of select genes. This finding is consistent with previous work demonstrating that the expression of only a specific subset of mRNAs—those with long and/or secondary-structured 5' UTRs—is reduced following *DDX3X/Ded1* disruption [50,51,77,78].

We next asked whether *DDX3X* regulates RAN translation on *FMR1* transcripts in other reading frames. The expression of the +2 (CGG)<sub>100</sub> NL-3xF RAN product (FMRpolyA<sub>100</sub>), which likely derives from initiation within the NRE [31], was reduced to a similar degree as the FMRpolyG<sub>100</sub> product in luminescence assays (Fig 3B and C; Appendix Fig S5B and C). We also observed these effects following detection of the FMRpolyG<sub>n</sub> and FMRpolyA<sub>n</sub> RAN products by

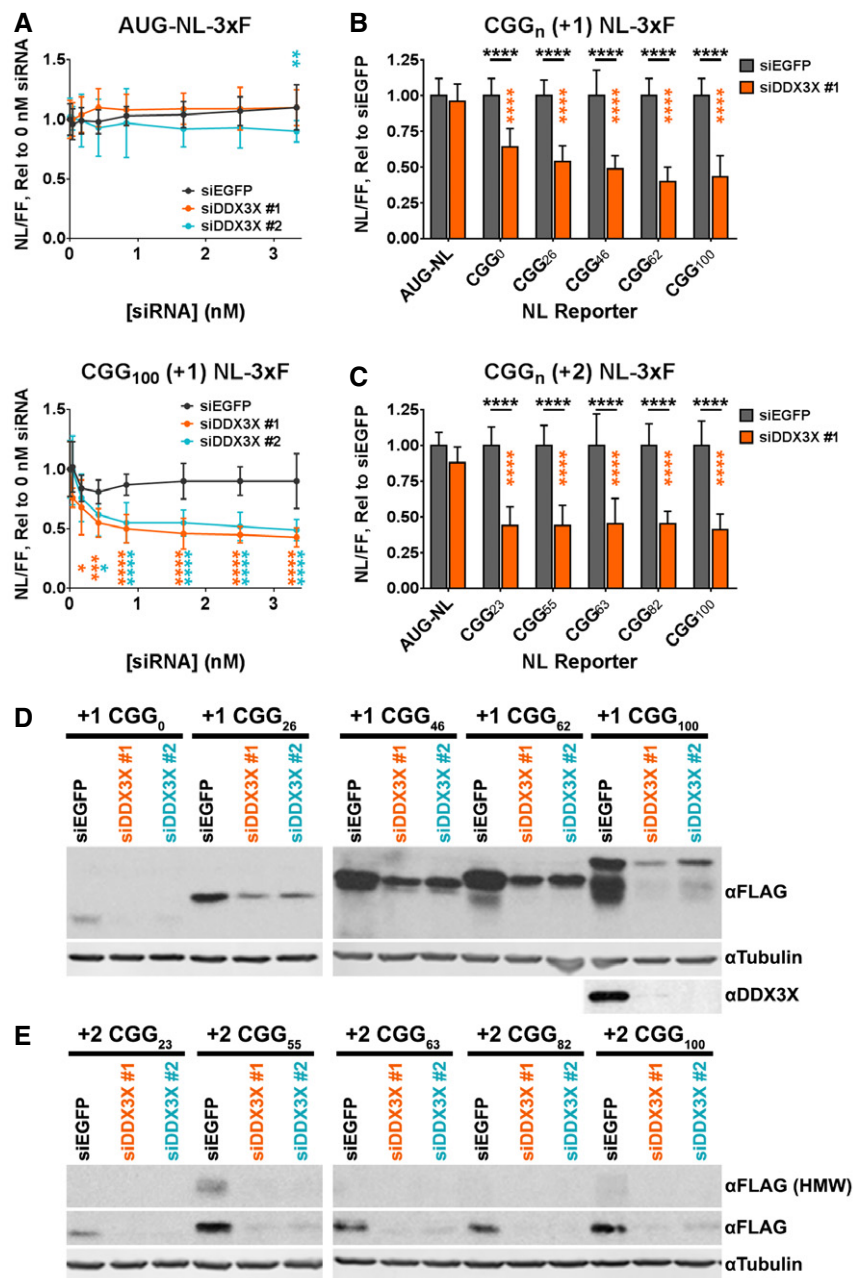


**Figure 3. Knockdown of *DDX3X* inhibits RAN translation in cultured human cells.**

**A** Dose–response curves showing the effects of two independent anti-*DDX3X* siRNAs on the expression of AUG-NL-3xF (top) and (CGG)<sub>100</sub> +1 NL-3xF (bottom) reporters. Plasmid-based reporters were transfected into HeLa cells 24 h after knockdown, and reporter expression was quantified by luminescence. Nanoluciferase (NL) luminescence has been normalized to luminescence from firefly luciferase (FF), which was co-transfected, in order to control for transfection variability. Asterisks refer to comparisons between anti-*DDX3X* siRNAs and siRNAs against EGFP (siEGFP; two-way ANOVA with Dunnett's multiple comparisons test;  $n = 12$ /condition). **B, C** (CGG)<sub>n</sub> +1 and (CGG)<sub>n</sub> +2 NL-3xF expression (normalized to FF) with and without *DDX3X* knockdown across a range of CGG repeat sizes. Black asterisks refer to comparisons between siDDX3X- and siEGFP-treated cells; orange asterisks refer to comparisons between siDDX3X-treated cells expressing AUG-NL-3xF and those expressing a different reporter (two-way ANOVA with Tukey's multiple comparisons test;  $n = 17$ –30/condition). **D, E** Western blots of FMRpolyG-NL-3xF and FMRpolyA-NL-3xF products with and without *DDX3X* knockdown across a range of repeat sizes. Data information: For all panels, \* $P \leq 0.05$ , \*\* $P \leq 0.01$ , \*\*\* $P \leq 0.001$ , \*\*\*\* $P \leq 0.0001$  for the specified statistical test. All panels depict data as means  $\pm$  SD (compiled from  $\geq 3$  replicates).

Western blotting (Fig 3D and E). These data indicate that the function of *DDX3X* in promoting RAN translation is not limited to a single reading frame.

*DDX3X* and its homologs in yeast and *Drosophila* function in several aspects of RNA metabolism. We therefore asked whether *DDX3X* functions in RAN translation directly or whether its effects

might instead be mediated by modulating RNA stability or transcription. Knockdown of *DDX3X* reduces the expression of +1 and +2 (CGG)<sub>100</sub> NL-3xF, regardless of whether the reporters are transfected as plasmids or *in vitro*-transcribed RNAs (Fig 4A; Appendix Fig S5D and E), suggesting that *DDX3X* acts post-transcriptionally. We next asked whether *DDX3X* knockdown impacted the abundance of reporter mRNAs following plasmid transfection. We observed that the mRNA abundance of both AUG-NL-3xF and (CGG)<sub>100</sub>-NL-3xF in the +1 and +2 frames was not consistently affected after transfection with siDDX3X #1 and siDDX3X #2 (Fig 4B). In order to isolate translational effects *per se* from other, concurrent effects on gene expression, we conducted *in vitro* translation assays using transcribed reporter RNAs and cytoplasmic extracts generated from cells depleted of *DDX3X* by two independent siRNAs. *DDX3X*-depleted extracts yielded reduced translation of +1 (CGG)<sub>100</sub> NL-3xF, while having either no effect on or increasing the synthesis of an AUG-NL-3xF reporter (Fig 4C). This effect was consistent across independently prepared *in vitro* translation extract replicates (four extracts per siRNA; two anti-*DDX3X* siRNAs, Appendix Fig S7A and B). These *in vitro* experiments point specifically to a direct translational function of *DDX3X*, while leaving open the possibility that changes in mRNA stability and abundance may further impact the expression of RAN products.

We next asked how *DDX3X* regulates *FMR1* RAN translation. To determine whether *DDX3X* can directly interact with CGG reporter mRNAs, we performed photo-crosslinking RNA immunoprecipitation (RIP) assays to probe for an interaction between *DDX3X* and our *FMR1* (CGG)<sub>100</sub> reporters in cultured cells. As we anticipated, significantly more *HSPA1A* mRNA (translation of which requires *DDX3X*) [52] was co-purified using antibodies against *DDX3X* than isotype control IgG (Fig 4D). Similarly, significantly more +1 (CGG)<sub>100</sub> NL-3xF mRNA was co-purified using antibodies against *DDX3X* than antibodies against EGFP or isotype control IgG (Fig 4D; Appendix Fig S8A). +1 (CGG)<sub>100</sub> NL-3xF mRNA was also enriched by *DDX3X* RIP in comparison with endogenous *MALAT* RNA, indicating a transcript-selective interaction between *DDX3X* and +1 (CGG)<sub>100</sub> NL-3xF mRNA. To determine whether that interaction is an artifact of the NL-3xF tag on +1 (CGG)<sub>100</sub> NL-3xF mRNA, we repeated the experiment using a 3'-truncated "tagless" construct in which the NL-3xF tag had been deleted (leaving the *FMR1* 5' UTR and minimal vector sequence intact). In two independent replicates, tagless (CGG)<sub>100</sub> mRNA also co-precipitated with *DDX3X*, near or above the levels of *HSPA1A* mRNA as a positive control (Appendix Fig S8B). Finally, to determine whether that interaction depends on the expanded CGG repeats in the tagless (CGG)<sub>100</sub> construct, we repeated this experiment using a modified tagless construct bearing 0 CGG repeats [tagless (CGG)<sub>0</sub>]. (CGG)<sub>0</sub> mRNAs co-precipitated with *DDX3X* at levels comparable to (CGG)<sub>100</sub> and *HSPA1A* mRNA, indicating that expanded CGG repeats are unnecessary for this interaction. This is not surprising, however, as the 5'UTR of *FMR1* is highly GC-rich (76%) even excluding the CGG NRE, and previously published work has demonstrated that *Ded1* (the yeast homolog of *DDX3X*) preferentially binds 5' to secondary structures within 5' UTRs [77].

To determine which features of the *FMR1* 5'UTR enable *DDX3X* to modulate RAN translation, we first varied the size of the CGG NRE in our reporters. Using plasmid-based reporters, we observed no significant effect of CGG repeat size on the impact of *DDX3X*

knockdown in either the GGC (+1) frame or the GCG (+2) frame (Fig 3B–E; Appendix Fig S5B and C). All exhibited decreased expression as measured by luminescence assays and Western blotting. We observed similar results when we transfected reporters as *in vitro*-transcribed RNA (Appendix Fig S5D and E). These results indicate that expanded CGG repeats are unnecessary for *DDX3X* to modulate RAN translation initiating within the *FMR1* 5' UTR.

One of the unique features of RAN translation is its use of non-AUG codons for initiation. We therefore asked whether *DDX3X* facilitated RAN translation by regulating start codon selection. We first tested the effect of *DDX3X* knockdown on a modified +1 (CGG)<sub>100</sub> reporter, in which the major near-AUG codon (ACG) utilized for GGC (+1)-frame RAN translation had been removed and replaced with a nearby AUG (Appendix Fig S9) [31]. This change enhanced basal expression of the construct, but *DDX3X* knockdown still impaired AUG-(CGG)<sub>100</sub> (+1) NL-3xF expression (Fig 4E). Similarly, insertion of an AUG codon in a strong Kozak context 5' to the NRE in the GCG (+2) frame enhanced basal expression, but the expression of this AUG-(CGG)<sub>100</sub> (+2) NL-3xF reporter remained *DDX3X*-dependent (Fig 4E). In a complementary experiment, we evaluated whether *DDX3X* knockdown affected translation of NL-3xF reporters that initiate with the near-cognate codons CUG, GUG, UUG, or ACG absent any NRE or *FMR1* sequence. As expected, the expression of CUG-, GUG-, UUG-, and ACG-NL-3xF reporter plasmids was lower than the expression of AUG-NL-3xF [30,37]. When these plasmids were transfected into cells, *DDX3X* knockdown reduced their expression compared to AUG-NL-3xF but significantly less than +1 (CGG)<sub>100</sub> NL-3xF (Fig 4F). In contrast, the expression of *in vitro*-transcribed near-AUG-initiated NL-3xF reporters was unaffected by *DDX3X* depletion in *in vitro* translation assays (Fig 4G; Appendix Fig S7C). In total, our results indicate that altered start codon fidelity is unlikely to be the sole factor mediating the effects of *DDX3X* knockdown on *FMR1* RAN translation.

#### eIF4B and eIF4H modulate RAN Translation at CGG repeats

eIF4B and eIF4H are co-stimulatory factors for the RNA helicase eIF4A, and like Belle/*DDX3X*, they are required for translation of mRNAs with long or structured 5' UTRs [50,53–55]. Previous work demonstrated that eIF4A is specifically required for RAN translation at both CGG repeats and GGGGCC repeats associated with ALS/FTD [30–32]. We therefore asked whether these co-stimulatory factors might play a similar, specific function in RAN translation like *DDX3X*. In our initial *Drosophila* screen, three shRNAs against *eIF4H1*, one shRNA against *eIF4H2*, and one shRNA against *eIF4B* suppressed the rough-eye phenotype induced by (CGG)<sub>90</sub>-EGFP (Fig 5A and B; Appendix Fig S10A and B). In addition, *eIF4B* over-expression exacerbated this phenotype, while having no effect in the absence of (CGG)<sub>90</sub>-EGFP (Appendix Fig S10C and D). As with *belle* shRNAs, these effects were not limited to the eye, as *eIF4B* shRNA increased and over-expression decreased the lifespan of flies expressing (CGG)<sub>90</sub>-EGFP under an inducible Tub5 driver (Appendix Fig S10E). These experiments suggest that, like Belle/*DDX3X*, eIF4B and eIF4H are capable of modulating RAN translation.

In contrast to Belle/*DDX3X*, the impact of modulating eIF4B or eIF4H expression was not specific to RAN translation. In cultured HeLa cells, knockdown of either *EIF4B* or *EIF4H* (Appendix Fig

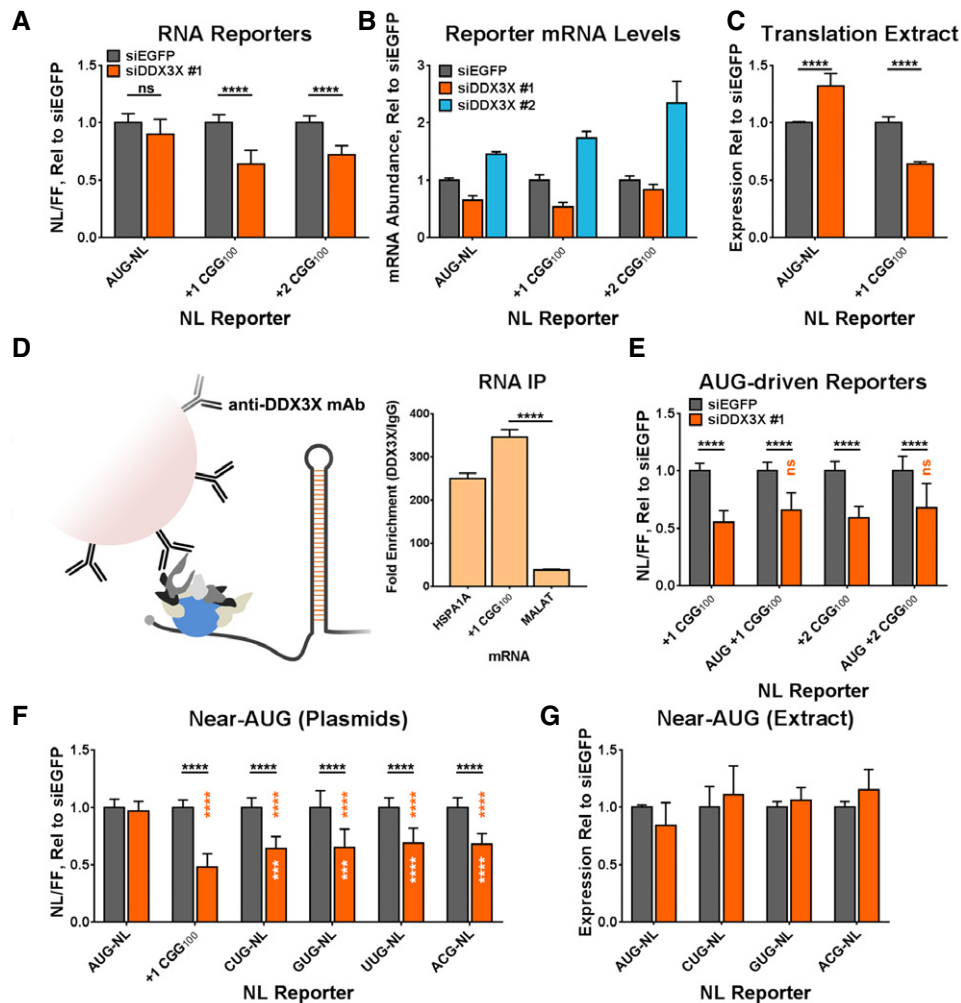


**Figure 4. DDX3X facilitates expression of RAN products at the level of translation.**

- A The expression of *in vitro*-transcribed AUG, +1 (CGG)<sub>100</sub>, and +2 (CGG)<sub>100</sub> NL-3xF RNAs following *DDX3X* knockdown in HeLa cells, expressed as NL luminescence normalized to FF luminescence. (Student's *t*-test with Bonferroni corrections for multiple comparisons; *n* = 21/condition).
- B Abundance of reporter mRNAs following *DDX3X* knockdown and plasmid-reporter transfection, determined by qRT-PCR (*n* = 7/condition). This panel depicts data as means ± SEM.
- C The expression of AUG-NL-3xF and +1 (CGG)<sub>100</sub> NL-3xF in *in vitro* translation extracts, collected from HeLa cells treated with siRNAs against EGFP or *DDX3X* (two-way ANOVA with Tukey's multiple comparisons test; *n* = 4/condition).
- D Enrichment of *HSPA1A* and +1 (CGG)<sub>100</sub> NL-3xF mRNA following anti-*DDX3X* RIP, relative to incubation with isotype control IgG. *MALAT* RNA, in contrast, is not enriched (Student's *t*-test, *n* = 3). Data from the additional replicate are presented in Appendix Fig S8A.
- E The expression of +1 and +2 (CGG)<sub>100</sub> NL-3xF plasmid reporters with and without an AUG inserted 5' to the CGG repeat, with and without *DDX3X* knockdown. Black asterisks refer to comparisons between siDDX3X- and siEGFP-treated cells; orange asterisks refer to comparisons between siDDX3X-treated cells expressing either +1 or +2 (CGG)<sub>100</sub> NL-3xF and those expressing the respective AUG-driven variant (two-way ANOVA with Tukey's multiple comparisons test; *n* = 11–12/condition).
- F The expression of NL-3xF plasmids with initiator AUG codons mutated to near-AUG codons, with and without *DDX3X* knockdown (two-way ANOVA with Dunnett's multiple comparisons test; *n* = 18–24/condition). Black asterisks refer to comparisons between siEGFP-treated and siDDX3X-treated cells; orange asterisks refer to comparisons between siDDX3X-treated cells expressing AUG-NL-3xF and those expressing a different reporter; white asterisks refer to comparisons between siDDX3X-treated cells expressing +1 (CGG)<sub>100</sub> NL-3xF and those expressing a different reporter.
- G The expression of *in vitro*-transcribed near-AUG reporter RNAs in *in vitro* translation extracts, collected from HeLa cells treated with siRNAs against EGFP or *DDX3X*. Experiments with independent, replicate lysates are presented in Appendix Fig S7C (*n* = 4/group).

Data information: For all panels, ns = non-significant, \*\*\**P* ≤ 0.001, \*\*\*\**P* ≤ 0.0001 for the specified statistical test. All panels depict data as means ± SD, unless indicated otherwise (compiled from ≥ 3 replicates).

S10F) similarly decreased the expression of +1 CCG<sub>100</sub> NL-3xF and a co-transfected AUG-driven firefly luciferase (AUG-FF) reporter (Fig 5C and D), suggesting that we cannot separate the role of eIF4B/H in RAN translation from their functions in translation generally. In support of this interpretation, over-expression of *EIF4H*

alone, or both *EIF4B* and *EIF4H* together, significantly increased the expression of +1 CCG<sub>100</sub> NL-3xF and AUG-NL-3xF (Fig 5E). These data suggest that eIF4B and eIF4H both regulate RAN translation but do so in a manner that is not specific to transcripts that are RAN translated.

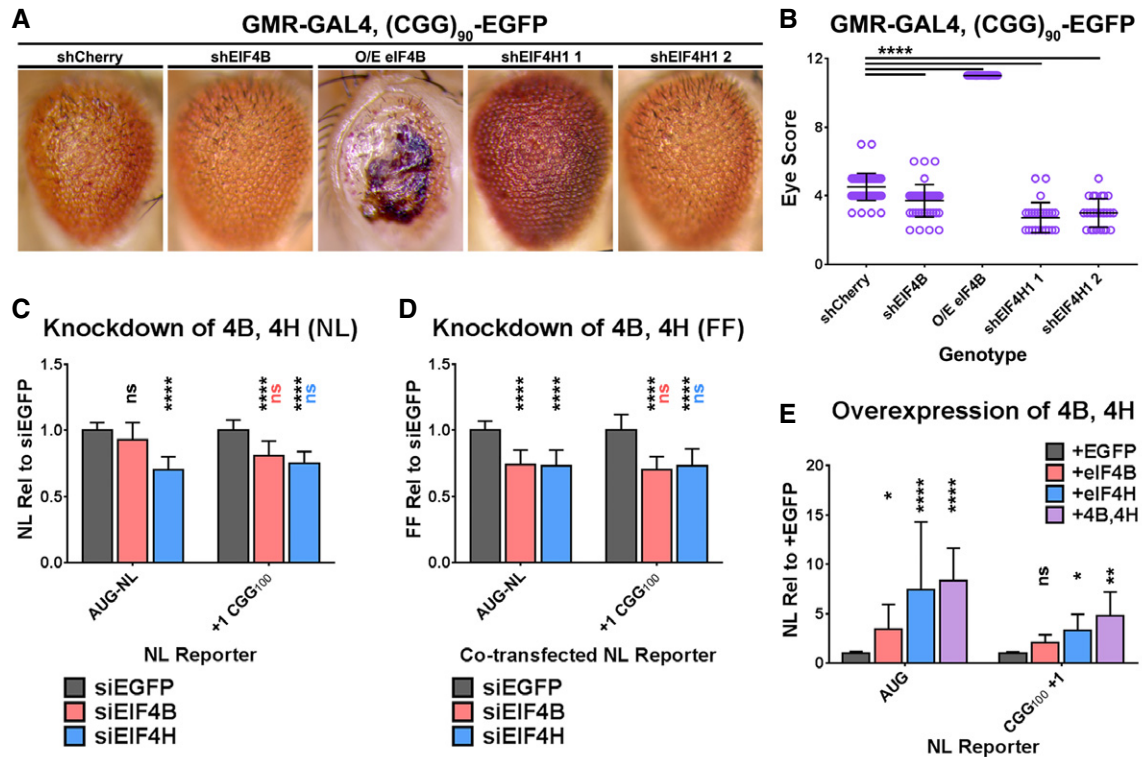


**Figure 5.** *EIF4B* and *EIF4H* modulate RAN translation and general translation in *Drosophila* and cultured human cells.

- A Representative photographs of GMR-GAL4; (CGG)<sub>90</sub>-EGFP fly eyes expressing manipulations of *eIF4B* and *eIF4H*.
- B Quantitation of GMR-GAL4, (CGG)<sub>90</sub>-EGFP eye phenotypes with *eIF4B/H* manipulations (Mann–Whitney *U*-test with Bonferroni corrections for multiple comparisons; *n* = 26–55/genotype).
- C, D The expression of plasmid-based AUG-NL and +1 (CGG)<sub>100</sub> NL-3xR reporters (C), or co-transfected AUG-FF reporters (D), following knockdown of *EIF4B* or *EIF4H*. Black asterisks refer to comparisons between siEGFP- and siEIF4B/H-treated cells; pink and blue asterisks refer to comparisons between siEIF4B- (pink) or siEIF4H- (blue) treated cells expressing AUG-NL-3xR and those expressing +1 (CGG)<sub>100</sub> (two-way ANOVA with Tukey's multiple comparisons test, *n* = 9/condition).
- E The expression of plasmid-based AUG-NL-3xR and (CGG)<sub>100</sub> +1 NL-3xR reporters with and without over-expression of *EIF4B*, *EIF4H*, or both (two-way ANOVA with Dunnett's multiple comparisons test; *n* = 20/condition). Asterisks refer to comparisons between cells over-expressing either EGFP or *EIF4B*, *EIF4H*, or *EIF4B* and *EIF4H* and expressing the same reporter.

Data information: For all panels, ns = non-significant, \**P* ≤ 0.05, \*\**P* ≤ 0.01, \*\*\*\**P* ≤ 0.0001 for the specified statistical test. All panels present data as means ± SD (compiled from ≥ 3 replicates).

### *eIF1* and *eIF5* modulate RAN translation in human cells via start codon selectivity

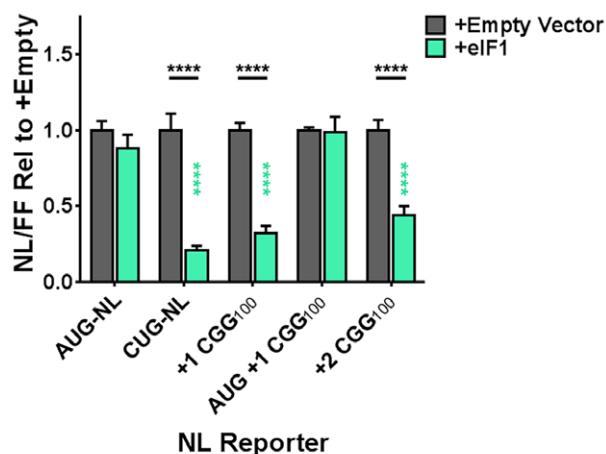
By definition, RAN translation follows a failure in start codon fidelity. Therefore, we predict that eIFs that enhance start codon fidelity would suppress RAN translation, while eIFs that reduce start codon fidelity would enhance RAN translation. We and others have pursued this concept in the context of the integrated stress response [30,32,39]: Cellular stressors trigger phosphorylation of eIF2 $\alpha$ , which suppresses global protein translation by reducing ternary complex (eIF2 $\alpha$ -GTP-tRNA<sup>Met</sup>) recycling and availability. Cellular stressors and mutations in multiple eIF2 subunits have both been shown to enhance initiation at non-AUG codons in yeast and mammalian cells [79,80]. Consistent with this, we and others observed that exogenous stressors or eIF2 $\alpha$  phosphorylation selectively enhances RAN translation at both CGG repeats and GGGGCC repeats associated with ALS [30,32,39] in a near-AUG codon-dependent manner. Several other eIFs are known to modulate start codon fidelity [33,81]. eIF1 maintains the fidelity of scanning 43S PICs

for AUG start codons by antagonizing the structural reconfigurations that follow AUG recognition [58,60–63]. We therefore asked whether *EIF1* over-expression might impact RAN translation. Over-expression of *EIF1* in cultured human cells decreased the expression of (CGG)<sub>100</sub> NL-3xR in the +1 and +2 frames (Fig 6A). Notably, inserting an AUG codon upstream of the CGG NRE in the +1 frame abolished this effect, indicating that the identity of the start codon is essential for modulation by eIF1. This demonstrates that manipulation of the molecular machinery that determines start codon fidelity can modulate RAN translation at CGG repeats in human cells.

We next asked whether siRNA-mediated *EIF1* knockdown would modulate RAN translation, and we observed that *EIF1* knockdown resulted in significant inhibition of all transfected reporters (Appendix Fig S11A). This finding is consistent with the known scanning-promoting functions of eIF1 during general translation initiation [61,62] and potentially explains the toxicity we observed with some *EIF1*-disrupting *Drosophila* lines in the absence of (CGG)<sub>90</sub>-EGFP (Appendix Fig S1), as well as the reduced



## A Overexpression of eIF1



## B Overexpression of eIF5

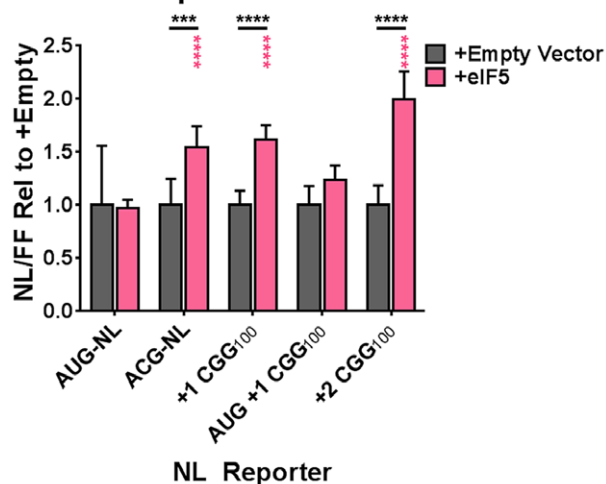


**Figure 6. *EIF1* and *EIF5* modulate RAN translation by determining AUG start codon specificity.**

A The expression of plasmid-based NL-3xF reporters in HEK293 cells with and without over-expression of *EIF1* (two-way ANOVA with Sidak's multiple comparisons test;  $n = 9-12$ /condition). Black asterisks refer to comparisons between empty vector-transfected and *EIF1*-transfected cells; green asterisks refer to comparisons between *EIF1*-transfected cells expressing AUG-NL-3xF and those expressing a different reporter.

B The expression of plasmid-based NL-3xF reporters in HEK293 cells with and without over-expression of *EIF5* (two-way ANOVA with Sidak's multiple comparisons test;  $n = 9-12$ /condition). Black asterisks refer to comparisons between empty vector-transfected and *EIF5*-transfected cells; pink asterisks refer to comparisons between *EIF5*-transfected cells expressing AUG-NL-3xF and those expressing a different reporter.

Data information: For all panels,  $***P \leq 0.001$ ,  $****P \leq 0.0001$  for the specified statistical test. Bars represent mean  $\pm$  SEM (compiled from  $\geq 3$  replicates).

(CGG)<sub>90</sub>-elicited toxicity we observed with *EIF1*-disrupting lines that were not, on their own, toxic.

We next asked whether enhancing expression of eIF5 would affect RAN translation. eIF5 is an eIF2 $\gamma$ -specific GTPase-activating protein (GAP) [82,83]. Once a 43S PIC recognizes a start codon,

eIF1 dissociates from the PIC, and eIF5 promotes the hydrolysis of eIF2 $\gamma$ -bound ATP [84–87], a critical step in the dissociation of other eIFs that must precede ribosomal subunit joining. Furthermore, Loughran *et al* [88] demonstrated that higher eIF5 abundance leads to increased initiation at non-AUG codons. Consistent with these results, we observed that *EIF5* over-expression in cultured human cells led to higher expression of ACG-initiated NL-3xF and +1 and +2 (CGG)<sub>100</sub> NL-3xF reporter plasmids, but not AUG-NL-3xF or AUG-initiated +1 (CGG)<sub>100</sub> NL-3xF reporters (Fig 6B). Moreover, we confirmed by Western blot that transfection of *EIF1* and *EIF5* cDNA-containing plasmids resulted in a higher level of eIF1 and eIF5 expression (Appendix Fig S11B). In total, these experiments demonstrate that manipulation of factors that influence start codon fidelity can up- or down-regulate RAN translation at CGG repeats.

### Knockdown of *DDX3X* suppresses toxicity in (CGG)<sub>100</sub>-expressing primary neurons

The toxicity of the CGG NRE in *FMR1* is driven at least in part by the products of RAN translation [14,17,18]. Having demonstrated that *DDX3X* regulates the abundance of RAN products in mammalian cells, we asked whether knockdown of *DDX3X* can mitigate the toxicity of (CGG)<sub>100</sub> repeats in mammalian neurons. We transfected primary rat neurons with locked nucleic acids (LNAs) against *DDX3X* or non-targeting controls, along with plasmids containing the human *FMR1* 5' UTR with 100 CGG repeats upstream of an EGFP reporter in the +1 frame [+1 (CGG)<sub>100</sub> EGFP], along with an AUG-driven mApple construct to highlight transfected cells. Over the following 10 days, we used automated longitudinal fluorescence microscopy to track the survival of transfected cells (Fig 7A) [89–91]. The expression of +1 (CGG)<sub>100</sub> EGFP markedly reduced neuronal survival compared to neurons expressing either EGFP (Appendix Fig S12) or an EGFP reporter in which the AUG start codon has been replaced with a GGG codon (GGG-EGFP). Knockdown of *DDX3X* (Fig 7B) by two independent LNAs reduced the expression of FMRpolyG<sub>100</sub>-EGFP in these neurons (Fig 7C) and significantly improved the survival of (CGG)<sub>100</sub>-expressing neurons relative to transfection of non-targeting control LNAs (Fig 7D and E). We observed some neurotoxicity with one of the LNA-targeted *DDX3X* (#2) but not the other, potentially indicative of adverse off-target effects from LNA #2. These findings suggest that, like in *Drosophila*, knockdown of *DDX3X* suppresses CGG NRE-elicited toxicity by inhibiting RAN translation.

## Discussion

We performed a screen of eIFs and RNA helicases to identify modifiers of *FMR1* NRE-associated RAN translation and toxicity in *Drosophila* and human cells, and found both selective (*bel/DDX3X*, *EIF1*, and *EIF5*) and non-selective (*EIF4B* and *EIF4H*) modifiers. Manipulation of these genes both reduced the expression of the RAN products FMRpolyG and FMRpolyA and mitigated CGG repeat-associated toxicity. This work both extends our understanding of RAN translation mechanisms and identifies potential therapeutic targets for FXTAS and potentially other RAN translation-associated disorders.

RAN translation occurs in association with expanded, GC-rich, secondary structure-forming repeats that promote initiation in the

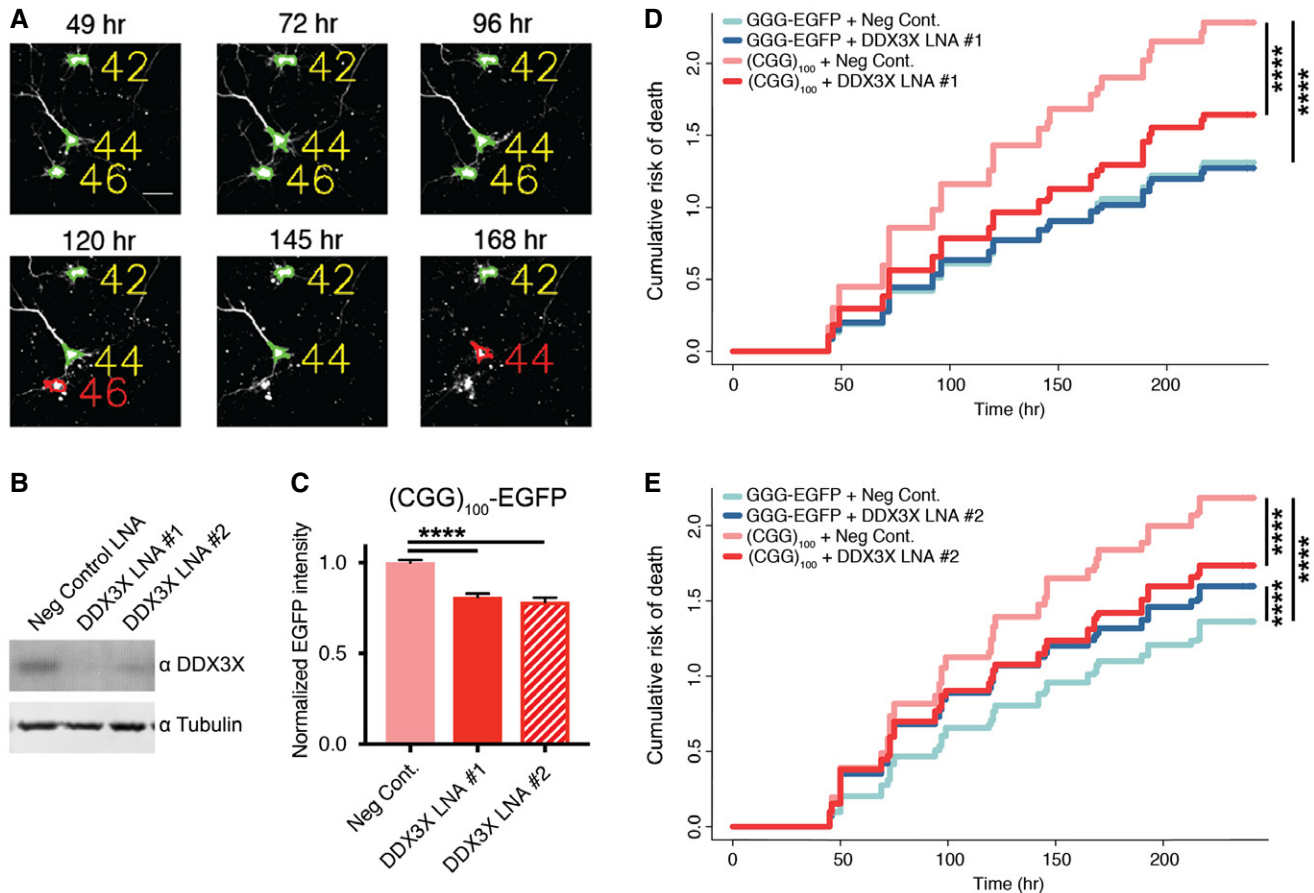


**Figure 7. Knockdown of *DDX3X* mitigates  $(CGG)_{100}$  toxicity in primary rodent neurons.**

- A Sample micrographs collected by automated longitudinal fluorescence microscopy, demonstrating the automated determination of cell death.
- B Anti-*DDX3X* Western blot of B35 cells transfected with either of two independent anti-*DDX3X* LNAs or a control LNA.
- C The expression of EGFP in primary rat neurons transfected with  $(CGG)_{100}$  (+1) EGFP and either anti-*DDX3X* LNAs or a control (one-way ANOVA with Tukey's multiple comparisons test;  $n = 2,408$ – $5,689$  cells/condition). All graphs depict pooled data, normalized first within the replicate.
- D, E Transfection of anti-*DDX3X* LNA #1 (D) or #2 (E) reduced the cumulative risk of death in  $(CGG)_{100}$  (+1) EGFP-expressing neurons (Cox proportional hazard analysis;  $n = 2,408$ – $3,676$  cells/condition).

Data information: For all panels, \*\*\*\* $P \leq 0.0001$  for the specified statistical test (compiled from  $\geq 3$  replicates).

absence of an AUG codon [10,14,31]. We originally hypothesized that disruption of RNA helicases, which resolve RNA–RNA secondary structures, would enhance RAN translation at CGG repeats. Our results demonstrated the opposite: Knockdown of *bel/DDX3X*, *EIF4B*, or *EIF4H* inhibited FMR1 RAN translation. How can we account for this discrepancy? *DDX3X* and its yeast homolog *Ded1* are DEAD-box RNA helicases that are required for resolution of RNA–RNA structures in long, GC-rich 5' UTRs of particular genes [46–52,77,92,93]. The *FMR1* 5' UTR is GC-rich (76%) independent of the CGG repeats and is predicted to form highly stable secondary structures [94–96] capable of stalling scanning 43S PICs [35,36]. Our results, in which *DDX3X* is required for initiation within the *FMR1* 5' UTR but not for expression of AUG-NL-3xF, are most consistent with a model in which *DDX3X* interacts with and resolves RNA–RNA secondary structures within the *FMR1* 5' UTR 5' to and within the CGG repeat, which allows access of scanning PICs to sites of initiation. Without *DDX3X*, scanning 43S PICs are unable to access the initiation sites for RAN translation, leading to a selective

decrease in their use. In contrast, *EIF4B* and *EIF4H* are stimulatory factors [53–55,97,98] for the DEAD-box RNA helicase eIF4A, which is critical for 43S PIC-mRNA binding and PIC scanning [50]. Our data, in which eIF4B and eIF4H regulate not only RAN translation but also general translation, are best explained with a model in which eIF4B and eIF4H facilitate 43S PIC attachment and basal scanning in the initial stages of RAN translation in a similar fashion to that for canonical translation. This model is consistent with previous observations that FMR1 RAN translation resembles canonical translation during these early stages of initiation [30–32].

A key feature that distinguishes RAN translation from canonical translation is its use of non-AUG codons for initiation [10,30–32]. The specificity for AUG start codons is simultaneously (and paradoxically) central to the integrity of eukaryotic and prokaryotic proteomes and an essential point of regulation for determining which, when, and how much protein is synthesized from a given mRNA transcript [81,99–102]. RNA secondary structure-forming elements (including GC-rich NREs) are predicted to slow or stall

PICs during scanning, enhancing the dwell time of codon-anticodon interactions at non-AUG codons and increasing the frequency of initiation events at non-AUG sites [37]. RAN translation might initiate in a similar manner. If correct, this model predicts that increasing the abundance of eIFs that boost start codon fidelity would inhibit RAN translation, while increasing abundance of eIFs that reduce start codon fidelity would enhance RAN translation. Multiple factors and regulatory pathways converge to govern start codon selection, including *EIF1* and *EIF5*. eIF1 (originally identified as Sui1) is known to increase the specificity of scanning 43S PICs for AUG start codons [58,103], while higher availability and abundance of eIF5 (originally Sui5) have been shown to decrease start codon fidelity [88,104,105].

Consistent with our prediction, we observed that *EIF1* over-expression decreased RAN translation in a start codon-dependent manner, while over-expression of *EIF5* did the opposite. However, as factors such as *EIF1* have multiple roles in translational initiation, suppression of their expression led to global decreases in translation that impacted both FMR1 RAN translation and canonical translation, which elicited intrinsic toxicity in *Drosophila*. These results align with previous work demonstrating that RAN translation at both CGG and GGGGCC NREs and across multiple reading frames is induced by activation of the ISR in a start codon-dependent manner via a mechanism that impinges on the AUG selectivity of the 43S PIC [30,34,39]. This line of research supports a model in which RAN translation represents a failure in start codon fidelity, suggesting that factors that regulate start codon fidelity also regulate this pathologic process.

A central goal of understanding how RAN translation occurs, and how it is distinct from canonical translation, is to identify potential therapeutic targets. Prevention of FMR1 RAN translation is sufficient to suppress toxicity/neurodegeneration in human cells *in vitro* and *Drosophila* and mice *in vivo* [14,17,18]. Here, we demonstrate that disruption of *bel/DDX3X* not only inhibits FMR1 RAN translation selectively *in vitro* and *in vivo*, but significantly mitigates repeat-induced toxicity across model systems. We suggest that targeting factors critical for resolving RNA secondary structures and/or enhancing start codon fidelity could represent viable therapeutic strategies for FXTAS and related neurodegenerative disorders. *DDX3X* in particular is currently the target of multiple lines of pharmacological research aimed at treating various cancers and viruses [106–108]. By targeting a proximal event in the pathophysiology of RAN translation-associated neurodegenerative disorders, this strategy has the potential to be more efficacious than targeting the toxic effects of each RAN product.

## Materials and Methods

### *Drosophila* lines

All fly lines used here and their sources are listed in Appendix Table S1.

### Antibodies

For Western blotting, all primary antibodies were used at 1:1,000 in 5% non-fat dairy milk (wt/vol), 0.02% NaN<sub>3</sub> (wt/vol), and 0.1%

Tween-20 (vol/vol) in TBS. Monoclonal mouse anti-EGFP antibody was acquired from Sigma (clones 7.1 and 13.1, catalog #11814460001). Monoclonal mouse anti- $\beta$ -tubulin antibody, developed by Michael Klymkowsky, was obtained from the Developmental Studies Hybridoma Bank, created by the NICHD of the NIH and maintained at The University of Iowa, Department of Biology, Iowa City, IA 52242. Monoclonal mouse anti-FLAG antibody was acquired from Sigma (clone M2, catalog #F1804). Polyclonal rabbit anti-DDX3X antibody (catalog #2635), anti-eIF4B antibody (catalog #3592), anti-eIF4H antibody (catalog #2444), anti-eIF1 antibody (catalog #12496), and anti-eIF5 antibody (catalog #13894) were acquired from Cell Signaling Technology. For information on the anti-DDX3X and isotype control antibodies used for RNA immunoprecipitation, see the relevant section below.

### *Drosophila* phenotyping

All flies were raised and crossed at 25°C on SY10 food unless otherwise stated. For the screen, virgin female flies carrying the UAS-*FMR1* (CGG)<sub>90</sub>-EGFP reporter [66] and a GMR-GAL4 driver [Bloomington *Drosophila* Stock Center (BDSC) 8605] were crossed to males carrying UAS-driven shRNA constructs against, UAS-driven transgenes of, or germline mutations in candidate genes. Rough-eye phenotypes in F<sub>1</sub> progeny were photographed and scored at 0–1 day post-eclosion according to a rubric adapted from Pandey *et al* [109]. One point was given for each of the following morphological aberrations: supernumerary inter-ommatidial bristles, abnormal orientation of inter-ommatidial bristles, disorganization of the ommatidial array, ommatidial fusion, and total loss of the ommatidial array over 10% of the eye surface. Two points were given for each of the following: the presence of necrotic lesions, collapse of the eye's convex surface, and shrinkage of the eye's surface area by 25%. Individual flies could therefore score between 0 and 11, with higher scores indicating a more severe phenotype. Eye images were captured using a Leica M125 stereomicroscope and a Leica DFC425 digital camera.

For longevity assays, flies carrying (CGG)<sub>90</sub>-EGFP and either a Tub5-GAL4 GeneSwitch or ElaV-GAL4 GeneSwitch driver (both RU486-inducible) [76] were placed on SY10 food supplemented with 200  $\mu$ M RU486 and flipped onto fresh RU486-supplemented SY10 every 24 (Tub5) or 48 (ElaV) h, and kept at 29°C until expiration. Deaths were counted and dead flies removed every 24 or 48 h.

### Western blotting and quantitative reverse-transcription-PCR (qRT-PCR) in *Drosophila*

For Western blotting and qRT-PCR of fly material, < 2 days post-eclosion flies carrying (CGG)<sub>90</sub>-EGFP and the Tub5-GAL4 GeneSwitch driver were placed on 200  $\mu$ M RU486-supplemented SY10 for 72 h, with fresh RU486-supplemented food provided every 24 h, at 29°C. For Western blotting, flies were homogenized at 4°C in ice-cold radioimmunoprecipitation assay (RIPA) buffer [50 mM Tris (pH 8.0), 150 mM NaCl, 0.1% SDS (wt/vol), 0.5% sodium deoxycholate (wt/vol), 1% IGEPAL CA-630 (vol/vol), and complete mini protease inhibitor (Roche)] and then centrifuged at 13,300 g for 2 min at 4°C to pellet cuticle and wing debris. The supernatant was removed and the chromatin sheared by 10 strokes through a 28.5G syringe. Lysates were subsequently mixed with 6 $\times$  reducing

Laemmli buffer, separated by SDS-PAGE, and transferred to PVDF membranes (Bio-Rad).

For qRT-PCR assays, flies were homogenized in TRIzol (Thermo Fisher Scientific) and total RNA was subsequently extracted. Ten micrograms of RNA per sample was twice incubated with 2 U of TURBO DNase (Thermo Fisher Scientific) in reaction volumes of 50  $\mu$ l at 37°C for 30 min, per manufacturer's instructions, and then recovered using RNA Clean and Concentrator-25 kits (Zymo Research). Five hundred nanograms of DNase-treated RNA per sample was used to generate cDNAs using a mixture of oligo(dT) and random hexamer primers (iScript cDNA Synthesis Kit, Bio-Rad). cDNA abundance was measured using iQ SYBR Green Supermix (Bio-Rad), appropriate primers at 300 nM (Appendix Table S2), and an iQ5 qPCR system (Bio-Rad).

### Plasmids

All reporter constructs used here were generated and described by Kearse *et al* [31] and/or Green *et al* [30]. In brief, all nanoluciferase reporters were developed by site-directed mutagenesis or digestion/ligation from pcDNA3.1(+)/AUG-NL-3xF. All pcDNA3.1(+)/*FMR1* (CGG)<sub>n</sub> NL-3xF constructs bear the full human 5' UTR of *FMR1* upstream of the CGG repeats. In addition, in every *FMR1* (CGG)<sub>n</sub> constructs used here, the initiator ATG of NL-3xF has been mutated to GGG to abolish initiation at this site. The firefly luciferase construct pGL4.13 was acquired from Promega. For *in vitro* transcription of firefly luciferase RNA, the firefly luciferase construct was digested and ligated into a pcDNA3.1(+) vector using 5' HindIII and 3' XbaI restriction sites (Rapid DNA Dephos and Ligation Kit, Sigma). All plasmids used for transfection and *in vitro* transcription were prepared from *Escherichia coli* cultures using ZymoPURE Plasmid Midiprep Kits (Zymo Research).

pCMV6-XL5/EIF4B and pCMV5-XL5/EIF4H, which drive expression of human *EIF4B* and *EIF4H*, respectively, were acquired from OriGene. pcDNA3.1(+)/EIF1 and pcDNA3.1D/EIF5-V5-His, which drive expression of human *EIF1* and *EIF5*, respectively, were acquired from J. Schofield.

### Cell culture and transfection

HeLa (CCL-2, ATCC), HEK293 (CRL-1573, ATCC), HEK293T (CRL-3216), and B35 (CRL-2754, ATCC) cells were cultured and passaged at 37°C, 5% CO<sub>2</sub>, with HeLa cells in Dulbecco's modified Eagle Medium (DMEM) supplemented with 10% fetal bovine serum (FBS) and 1% non-essential amino acids, and HEK293, HEK293T, and B35 cells in DMEM supplemented with 10% FBS.

For luciferase assays, HeLa cells were plated in 96-well plates at  $1.0 \times 10^4$  cells/well in 100  $\mu$ l media and reverse transfected with Stealth siRNAs against human *DDX3X* (DDX3XHSS102712 and DDX3XHSS176054, Thermo Fisher Scientific) or EGFP at 1.67 nM, unless otherwise noted, using Lipofectamine RNAiMAX (Thermo Fisher Scientific). Alternatively, they were transfected with ON-TARGETplus SMARTpool siRNAs against human *EIF4B* (L-020179-00, Dharmacon), *EIF4H* (L-013054-00), or *EIF1* (L-015804-02) or a non-targeting pool (D-001810-10). In brief, siRNA and RNAiMAX were diluted in Opti-MEM, combined, incubated for 10 min at room temperature, and then mixed with cells. For subsequent plasmid transfection, 24 h after plating cells were transfected with 25 ng/well

pcDNA3.1(+)/NL-3xF plasmid and 25 ng/well firefly luciferase transfection control plasmid (pGL4.13) using jetPRIME (Polyplus). The transfection media was removed and replaced 4 h post-transfection. For RNA reporter transfection, 24 h after plating cells were transfected with 25 ng/well *in vitro*-transcribed nanoluciferase RNA and 25 ng/well firefly luciferase RNA using TransIT mRNA (Mirus Bio). Luciferase assays were performed 24 h after plasmid transfection, as described by Kearse *et al* [31] and Green *et al* [30].

For over-expression experiments, cells were plated in 96-well plates at  $1.0 \times 10^4$  cells/well (HeLa) or  $2.0 \times 10^4$  cells/well (HEK293T) in 100  $\mu$ l media. Twenty-four hours after plating, HeLa cells were transfected with 5 ng/well pcDNA3.1(+)/NL-3xF, 5 ng/well pGL4.13, and 40 ng/well pCMV6-XL5/EIF4B, pCMV5-XL5/EIF4H, pEGFP N1, or a combination thereof, using jetPRIME (Polyplus). HEK293T cells were transfected with 25 ng/well pcDNA3.1(+)/NL-3xF, 25 ng/well pGL4.13, and 250 ng/well pcDNA3.1(+)/EIF1, empty pcDNA3.1(+), pcDNA3.1D/V5-His-EIF5, or empty pcDNA3.1D/V5-His using FuGENE HD (Promega). Luciferase assays were performed as above.

For Western blotting experiments, HeLa cells were plated in 12-well plates at  $1.5 \times 10^5$  cells/well in 1 ml media and reverse transfected, as above, with Stealth siRNAs against *DDX3X* or EGFP at 1.67 nM using Lipofectamine RNAiMAX. Alternatively, they were transfected with ON-TARGETplus SMARTpool siRNAs against *EIF4B*, *EIF4H*, or a non-targeting pool at 15 nM. Twenty-four hours after plating, cells were transfected with 500 ng/well pcDNA3.1(+)/NL-3xF using jetPRIME (Polyplus). The transfection media was removed and replaced 4 h post-transfection. Twenty-four hours after plasmid transfection, cells were lysed on-plate in RIPA buffer. The lysate was homogenized by 10 strokes through a 28.5G syringe (without centrifugation), mixed with 6 $\times$  reducing Laemmli buffer, heated at 90°C for 10 min, resolved by SDS-PAGE, and transferred to a PVDF membrane before incubation in primary antibody.

For qRT-PCR experiments, HeLa cells were plated in 6-well plates at  $2.5 \times 10^5$  cells/well in 2.5 ml media and reverse transfected with Stealth siRNAs against *DDX3X* or EGFP at 1.67 nM using Lipofectamine RNAiMAX. Twenty-four hours after plating cells were transfected with 625 ng/well pcDNA3.1(+)/NL-3xF and 625 ng/well pGL4.13 using jetPRIME (Polyplus). The transfection media was removed and replaced 4 h post-transfection. Twenty-four hours after plasmid transfection, cells were lysed and total cellular RNA collected using Quick-RNA MiniPrep Kit (Zymo Research). Five micrograms of RNA per sample was incubated twice with 2 U of TURBO DNase (Thermo Fisher Scientific) for 30 min at 37°C to remove contaminating genomic and plasmid DNA, and then recovered using the RNA Clean and Concentrator-25 Kit (Zymo Research). cDNA was generated from 500 ng of DNase-treated RNA per sample and a mixture of oligo(dT) and random hexamer primers (iScript cDNA Synthesis Kit, Bio-Rad). cDNA abundance was measured using iQ SYBR Green Supermix (Bio-Rad), an iQ5 qPCR system (Bio-Rad), and the appropriate primers at 300 nM. cDNA abundance was quantified using a modified  $\Delta\Delta C_t$  method recommended by the manufacturer and was presented as normalized to spiked-in *in vitro*-transcribed RNAs to account for differences in RT efficiency.

For confirmation of anti-*DDX3X* locked nucleic acid (LNA) efficacy, B35 cells were plated in 12-well plates at  $2.0 \times 10^5$  cells/well in 1 ml media and reverse transfected with anti-*DDX3X* Silencer

Select LNAs (s165214 and s165216, Thermo Fisher Scientific) or a non-targeting control (4390843, Thermo Fisher Scientific) at 40 nM using Lipofectamine RNAiMAX. Forty-eight hours after plating, cells were lysed as above for Western blot analysis.

### Crosslinking and RNA immunoprecipitation

HEK293 cells were plated in poly-L-lysine-coated 10-cm plates at  $3.0 \times 10^6$  cells/plate. Forty-eight hours after plating, cells were transfected with 5  $\mu$ g of pcDNA3.1+/CGG<sub>100</sub> (+1) NL-3xF and 5  $\mu$ g of either pGL4.13 or pEGFP N1 using ViaFect (Promega). Twenty-four hours post-transfection, the media was aspirated and replaced with fresh media supplemented with 6-thioguanine (6SG) [110] at 100  $\mu$ M and allowed to incubate for 12 h.

Cells were rinsed 3 $\times$  in PBS (pH 7.4), the PBS was aspirated, and the cells were irradiated uncovered with 0.6 J/cm<sup>2</sup> of 365 nm UV light using a Stratalinker 2400 (Stratagene). Cells were then harvested using trypsin (0.25%)-EDTA and rubber policemen, collected by centrifugation, rinsed 2 $\times$  in PBS, flash-frozen in a dry ice/EtOH bath, and stored at  $-80^\circ\text{C}$ . For processing, cell pellets were lysed in NP-40 lysis buffer [50 mM Tris (pH 7.5), 150 mM NaCl, 1 mM DTT, 0.5% IGEPAL CA-630 (wt/vol)] supplemented with complete mini EDTA-free protease inhibitors (Roche), PhosSTOP phosphatase inhibitors (Roche), 1 U/ $\mu$ l recombinant RNasin (Promega), and 200 U/ml SuperaseIN (Thermo Fisher Scientific) for 25 min on ice, incubated with 42 U/ml RQ1 DNase (Promega) at 37°C for 10 min, and then centrifuged at 10,000 g, 4°C for 10 min.

Protein G Dynabeads (Thermo Fisher Scientific) were prepared and incubated with mouse anti-DDX3X (clone 2253C5a, Santa Cruz sc-81247), mouse anti-EGFP (clones 7.1/13.1, Sigma 11814460001), or mouse isotype control IgG (Thermo Fisher Scientific 10400C) as per the manufacturer's instructions. Antibody-conjugated beads were rinsed 3 $\times$  in NP-40 lysis buffer and incubated with the cleared lysate for 16 h with inversion at 4°C. Only those cells transfected with pEGFP N1 were subjected to anti-EGFP RIP. The lysate was removed, and the beads were washed 3 $\times$  with NP-40 lysis buffer and 3 $\times$  with 5 $\times$  PBS (pH 7.4) supplemented with 0.5% IGEPAL CA-630. RNA was eluted by incubation with 2 mg/ml proteinase K at 55°C for 1 h in 50 mM Tris-HCl (pH 7.0), 75 mM NaCl, 6 mM EDTA, and 2% SDS (wt/vol), extracted using TRIzol (Thermo Fisher Scientific) and GlycoBlue co-precipitant (Thermo Fisher Scientific), treated twice with 40 U/ml TURBO DNase at 37°C for 30 min, and purified using the RNA Clean and Concentrator-5 Kit (Zymo Research). cDNAs were generated using the iScript cDNA Synthesis Kit, as described above, with each reaction spiked with equal amounts of *in vitro*-transcribed AUG-FF or EGFP RNA (depending on which plasmid had not been co-transfected) as a reverse-transcription control. qPCR was performed as described above, with cDNA abundance normalized to FF or EGFP cDNA abundance.

### *In vitro* transcription and translation reactions

pcDNA3.1(+)/NL-3xF and pcDNA3.1(+)/FF were linearized by PspOMI and XbaI restriction enzymes (NEB), respectively, and recovered using DNA Clean and Concentrator-25 kits (Zymo Research). m<sup>7</sup>G-capped and poly-adenylated RNAs were transcribed *in vitro* from these plasmids using HiScribe T7 ARCA mRNA Kit (with tailing; NEB) as per the manufacturer's instructions and

recovered using RNA Clean and Concentrator-25 kits (Zymo Research). The integrity and size of all transcribed RNAs were confirmed by denaturing agarose gel electrophoresis with formaldehyde/formamide.

For preparation of translation-competent extracts, HeLa cells were plated in 14.5-cm dishes at  $8 \times 10^6$  cells/plate. Twenty-four hours later, they were forward transfected with Stealth siRNAs against DDX3X or EGFP at 1.67 nM using RNAiMAX, as described above (adapted from Rakotondrifara & Heintze [111]). The transfection media was removed 5 h post-transfection and replaced with fresh media. Two days post-transfection, cells were harvested using trypsin (0.25%)-EDTA, centrifuged, and rinsed 3 $\times$  with PBS (pH 7.4). Cells were allowed to swell on ice in a volume of hypotonic lysis buffer [10 mM HEPES-KOH (pH 7.6), 10 mM KOAc, 0.5 mM Mg<sub>2</sub>OAc, 5 mM DTT, supplemented with complete mini, EDTA-free protease inhibitor] equal to the cell pellet volume for 30 min. Cells were mechanically disrupted at 4°C using 20 strokes in a 27G syringe and then allowed to incubate on ice for an additional 20 min. Lysis was confirmed visually in > 95% of cells by trypan blue inclusion. The lysate was centrifuged at 10,000 g for 10 min at 4°C. The supernatant was then collected, diluted in lysis buffer to 8.0  $\mu$ g/ $\mu$ l using a modified Bradford protein quantification assay (Bio-Rad), flash-frozen in liquid N<sub>2</sub>, and stored at  $-80^\circ\text{C}$ .

For *in vitro* translation reactions, lysates were brought to final concentrations of 20 mM HEPES-KOH (pH 7.6), 44 mM KOAc, 2.2 mM Mg<sub>2</sub>AOC, 2 mM DTT, 20 mM creatine phosphate (Roche), 0.1  $\mu$ g/ $\mu$ l creatine kinase (Roche), 0.1 mM spermidine, and on average 0.1 mM of each amino acid (with relative amounts approximating those in eukaryotes) [112]. To this, *in vitro*-transcribed RNAs were added to 4 nM in a final volume of 10  $\mu$ l per reaction. After incubation at 30°C for 30 min, 25  $\mu$ l room temperature Glo Lysis Buffer (Promega) was added to halt the reaction and allowed to incubate for 5 min at room temperature. To 25  $\mu$ l of this mixture was added 25  $\mu$ l of Nano-Glo substrate freshly diluted in Nano-Glo buffer (Promega). This mixture was allowed to incubate in opaque 96-well plates on a rocking shaker in the dark for 5 min before the luminescence detection and quantification using a GloMax microplate luminometer (Promega).

### Polysome fractionation

HeLa cells were seeded in four to eight 10-cm dishes per condition. Twenty-four hours after plating, cells were transfected with siRNAs against DDX3X or EGFP at 1.6 nM using RNAiMAX, as above, with the media exchanged at 5 h post-transfection. When cells reached 70–90% confluent, 24–36 h post-knockdown, they were treated with 100  $\mu$ g/ml cycloheximide (CHX) for 5 min at 37°C. Cells were then transferred to ice and washed with 2.5 ml ice-cold PBS containing 100  $\mu$ g/ml CHX, collected by scraping in 2.5 ml cold PBS + CHX, and pelleted at 234 g and 4°C for 5 min. PBS was aspirated and pellets re-suspended in polysome-profiling lysis buffer (20 mM Tris-HCl (pH 7.5), 150 mM NaCl, 15 mM MgCl<sub>2</sub>, 8% (vol/vol) glycerol, 20 U/ml SUPERase, 80 U/ml murine RNase inhibitor, 0.1 mg/ml heparin, 100  $\mu$ g/ml CHX, 1 mM DTT, 1 $\times$  EDTA-free protease inhibitor cocktail, 20 U/ml Turbo DNase, 1% Triton X-100) [113]. Lysates were passed through a 20G needle 10 $\times$  and incubated on ice for 5 min. Cellular debris was pelleted at 14,000 g and 4°C for 5 min, and supernatant transferred to a fresh tube. Total lysate RNA

was estimated by NanoDrop. Lysates were flash-frozen in liquid N<sub>2</sub> and stored at  $-80^{\circ}\text{C}$  until fractionation.

Sucrose gradients were prepared by successively freezing equal volumes of 50, 36.7, 23.3, and 10% sucrose (wt/vol) in 12-ml Seton tubes. Sucrose-gradient buffer consisted of 20 mM Tris-HCl (pH 7.5), 150 mM NaCl, 15 mM MgCl<sub>2</sub>, 10 U/ml SUPERase, 20 U/ml murine RNase inhibitor, 100  $\mu\text{g/ml}$  CHX, and 1 mM DTT (Simsek *et al* [113]). Prior to use, gradients were allowed to thaw and linearize overnight at  $4^{\circ}\text{C}$  (Luthe, Analytical Biochemistry, 1983). For fractionation, approximately 90 (trial 1 with four 10-cm dishes), 220, and 250  $\mu\text{g}$  (trials 2 and 3, respectively, with eight 10-cm dishes) total RNA was applied to the top of the sucrose gradient. Gradients were spun at 151,263 g and  $4^{\circ}\text{C}$  for 3 h using a Beckman Coulter Optima L-90K ultracentrifuge and SW 41 Ti swinging-bucket rotor.

Gradients were fractionated with Brandel's Gradient Fractionation System, measuring absorbance at 254 nm. The detector was base-lined with 60% sucrose chase solution, and its sensitivity set to 0.5 for trial 1, and 1.0 for trials 2 and 3. For fractionation, 60% sucrose was pumped at a rate of 1.5 ml/min. Brandel's PeakChart software was used to collect data, overlay profiles, and calculate the area under the curve for monosome and polysome fractions.

### Primary neuronal cultures and automated fluorescence microscopy

Embryonic day (E) 19–20 Long-Evans rat (*Rattus norvegicus*) cortices were harvested and the neurons dissociated and plated in 96-well plates at  $6.0 \times 10^6$  cells/ml as previously described [114]. On *in vitro* day (DIV) 4, neurons were transfected using Lipofectamine 2000 (Thermo Fisher Scientific) [115] with 100 ng/well pGW/(CGG)<sub>100</sub> +1 EGFP or pGW/GGG-EGFP, 50 ng/well pGW/mApple, and LNAs to a final concentration of 40 nM. Following transfection, neurons were maintained in NEUMO photostable media (Cell Guidance Systems) for the length of the experiment.

Neurons were imaged using a Nikon Eclipse Ti inverted microscope with PerfectFocus3 and Nikon Plan Fluor 20 $\times$  objective lens [90]. Cells were illuminated with a Lambda XL Xenon lamp (Sutter Instrument) and detected using an Andor iXon3 897 EMCCD or Andor Zyla4.2 (+) sCMOS camera. Stage, filter, and shutter movements were controlled with scripts written in BeanShell for use in  $\mu$ Manager. Separate ImageJ/Fiji macros and Python scripts were employed for automated identification of transfected neurons and the drawing of regions of interest (ROIs) around each neuron [91]. Cell death was indicated by rounding of the cell body, deterioration of neuronal processes, and loss of mApple fluorescence intensity.

### Data analysis

Band intensity on Western blots was quantified using ImageJ (NIH; anti-EGFP) or Odyssey Image Studio (LI-COR; anti-tubulin) software. Primary neuron survival analysis and determination of hazard ratios through Cox proportional hazard analysis were conducted using the publicly available survival package in R. All other data were analyzed using GraphPad Prism 7.00.

**Expanded View** for this article is available online.

### Acknowledgements

We thank Scott Pletcher's lab at the University of Michigan for providing Tub5-GS and ElaV-GS lines and all fly food. We thank Peng Jin's lab at Emory University for providing the (CGG)<sub>90</sub>-EGFP line. We thank Wu-Min Deng's lab at Florida State University for providing mutant *belle* lines. We thank Ting Xie's lab at the University of Kansas for providing the UAS-eIF4A line. We thank J. Schofield for pcDNA3.1+/EIF1 and pcDNA3.1D/EIF5-V5-His plasmids. We thank David Turner for technical assistance with photo-crosslinking and RIP experiments. We thank Michael Kearse and everyone in the Todd lab for many thoughtful conversations and their collective wisdom. This work was funded by grants from the VA BLRD (1I21BX001841 and 1I01BX003231), the NIH (R01NS099280 and R01NS086810), and the Michigan Alzheimer's Disease Center and Protein Folding Disease Initiative to PKT. KMG, BNF, and AEL were supported by NIH T32GM007315. KMG was further supported by NIH F31NS100302 and AEL by NIH F30NS098571. MRG was supported by NIH T32NS007222-35S1. SJB and BNF were supported by the NIH (R01-NS097542, 1P30AG053760-01) and Ann Arbor Active Against ALS.

### Author contributions

AEL conceived the project, designed and performed experiments, analyzed and interpreted data, and wrote the article. FH helped conceive the project and design and perform experiments. AMM, MRG, BNF, AK, HCA, and KMG designed/performed experiments and analyzed/interpreted data. SN and SJF performed experiments. SJB provided necessary equipment, designed experiments, and interpreted data. PKT provided funding, conceived the project, designed experiments, interpreted data, and wrote the article.

### Conflict of interest

The authors declare that they have no conflict of interest.

### References

- Nelson DL, Orr HT, Warren ST (2013) The unstable repeats—three evolving faces of neurological disease. *Neuron* 77: 825–843
- La Spada AR, Paulson HL, Fischbeck KH (1994) Trinucleotide repeat expansion in neurological disease. *Ann Neurol* 36: 814–822
- Paulson HL, Perez MK, Trotter Y, Trojanowski JQ, Subramony SH, Das SS, Vig P, Mandel JL, Fischbeck KH, Pittman RN (1997) Intracellular inclusions of expanded polyglutamine protein in spinocerebellar ataxia type 3. *Neuron* 19: 333–344
- Paulson HL, Shakkottai VG, Clark HB, Orr HT (2017) Polyglutamine spinocerebellar ataxias – from genes to potential treatments. *Nat Rev Neurosci* 18: 613–626
- Warrick JM, Paulson HL, Gray-Board GL, Bui QT, Fischbeck KH, Pittman RN, Bonini NM (1998) Expanded polyglutamine protein forms nuclear inclusions and causes neural degeneration in *Drosophila*. *Cell* 93: 939–949
- Mankodi A, Urbinati CR, Yuan QP, Moxley RT, Sansone V, Krym M, Henderson D, Schalling M, Swanson MS, Thornton CA (2001) Muscleblind localizes to nuclear foci of aberrant RNA in myotonic dystrophy types 1 and 2. *Hum Mol Genet* 10: 2165–2170
- Miller JW, Urbinati CR, Teng-Umuay P, Stenberg MG, Byrne BJ, Thornton CA, Swanson MS (2000) Recruitment of human muscleblind proteins to (CUG)(n) expansions associated with myotonic dystrophy. *EMBO J* 19: 4439–4448
- Ranum LP, Cooper TA (2006) RNA-mediated neuromuscular disorders. *Annu Rev Neurosci* 29: 259–277

9. Jain A, Vale RD (2017) RNA phase transitions in repeat expansion disorders. *Nature* 546: 243–247
10. Zu T, Gibbens B, Doty NS, Gomes-Pereira M, Huguet A, Stone MD, Margolis J, Peterson M, Markowski TW, Ingram MA et al (2011) Non-ATG-initiated translation directed by microsatellite expansions. *Proc Natl Acad Sci USA* 108: 260–265
11. Ash PE, Bieniek KF, Gendron TF, Caulfield T, Lin WL, DeJesus-Hernandez M, van Blitterswijk MM, Jansen-West K, Paul III JW, Rademakers R et al (2013) Unconventional translation of C9ORF72 GGGGCC expansion generates insoluble polypeptides specific to c9FTD/ALS. *Neuron* 77: 639–646
12. Gendron TF, Bieniek KF, Zhang YJ, Jansen-West K, Ash PE, Caulfield T, Daugherty L, Dunmore JH, Castanedes-Casey M, Chew J et al (2013) Antisense transcripts of the expanded C9ORF72 hexanucleotide repeat form nuclear RNA foci and undergo repeat-associated non-ATG translation in c9FTD/ALS. *Acta Neuropathol* 126: 829–844
13. Mori K, Weng SM, Arzberger T, May S, Rentzsch K, Kremmer E, Schmid B, Kretzschmar HA, Cruts M, Van Broeckhoven C et al (2013) The C9orf72 GGGGCC repeat is translated into aggregating dipeptide-repeat proteins in FTLD/ALS. *Science* 339: 1335–1338
14. Todd PK, Oh SY, Krans A, He F, Sellier C, Frazer M, Renoux AJ, Chen KC, Scaglione KM, Basur V et al (2013) CGG repeat-associated translation mediates neurodegeneration in Fragile X tremor ataxia syndrome. *Neuron* 78: 440–455
15. Zu T, Liu Y, Banez-Coronel M, Reid T, Pletnikova O, Lewis J, Miller TM, Harms MB, Falchook AE, Subramony SH et al (2013) RAN proteins and RNA foci from antisense transcripts in C9ORF72 ALS and frontotemporal dementia. *Proc Natl Acad Sci USA* 110: E4968–E4977
16. Mizielińska S, Gronke S, Niccoli T, Ridler CE, Clayton EL, Devoy A, Moens T, Norona FE, Woollacott IOC, Pietrzyk J et al (2014) C9orf72 repeat expansions cause neurodegeneration in *Drosophila* through arginine-rich proteins. *Science* 345: 1192–1194
17. Sellier C, Buijssen RAM, He F, Natla S, Jung L, Tropel P, Gaucherot A, Jacobs H, Meziane H, Vincent A et al (2017) Translation of expanded CGG repeats into FMRpolyG is pathogenic and may contribute to Fragile X tremor ataxia syndrome. *Neuron* 93: 331–347
18. Buijssen RA, Visser JA, Kramer P, Severijnen EA, Gearing M, Charlet-Berguerand N, Sherman SL, Berman RF, Willemsen R, Hukema RK (2016) Presence of inclusions positive for polyglycine containing protein, FMRpolyG, indicates that repeat-associated non-AUG translation plays a role in Fragile X-associated primary ovarian insufficiency. *Hum Reprod* 31: 158–168
19. Zu T, Pattamatta A, Ranum LPW (2018) Repeat-associated Non-ATG translation in neurological diseases. *Cold Spring Harb Perspect Biol* 10: a033019
20. Banez-Coronel M, Ayhan F, Tarabochia AD, Zu T, Perez BA, Tusi SK, Pletnikova O, Borchelt DR, Ross CA, Margolis RL et al (2015) RAN translation in huntington disease. *Neuron* 88: 667–677
21. Hagerman PJ, Hagerman RJ (2015) Fragile X-associated tremor/ataxia syndrome. *Ann N Y Acad Sci* 1338: 58–70
22. Iwahashi CK, Yasui DH, An HJ, Greco CM, Tassone F, Nannen K, Babineau B, Lebrilla CB, Hagerman RJ, Hagerman PJ (2006) Protein composition of the intranuclear inclusions of FXTAS. *Brain* 129: 256–271
23. Jin P, Duan R, Qurashi A, Qin Y, Tian D, Rosser TC, Liu H, Feng Y, Warren ST (2007) Pur alpha binds to rCGG repeats and modulates repeat-mediated neurodegeneration in a *Drosophila* model of Fragile X tremor/ataxia syndrome. *Neuron* 55: 556–564
24. Muslimov IA, Patel MV, Rose A, Tiedge H (2011) Spatial code recognition in neuronal RNA targeting: role of RNA-hnRNP A2 interactions. *J Cell Biol* 194: 441–457
25. Sellier C, Freyermuth F, Tabet R, Tran T, He F, Ruffenach F, Alunni V, Moine H, Thibault C, Page A et al (2013) Sequestration of DROSHA and DGCR25 by expanded CGG RNA repeats alters microRNA processing in fragile X-associated tremor/ataxia syndrome. *Cell Rep* 3: 869–880
26. Sellier C, Rau F, Liu Y, Tassone F, Hukema RK, Gattoni R, Schneider A, Richard S, Willemsen R, Elliott DJ et al (2010) Sam68 sequestration and partial loss of function are associated with splicing alterations in FXTAS patients. *EMBO J* 29: 1248–1261
27. Sofola OA, Jin P, Qin Y, Duan R, Liu H, de Haro M, Nelson DL, Botas J (2007) RNA-binding proteins hnRNP A2/B1 and CUGBP1 suppress Fragile X CGG premutation repeat-induced neurodegeneration in a *Drosophila* model of FXTAS. *Neuron* 55: 565–571
28. Glineburg MR, Todd PK, Charlet-Berguerand N, Sellier C (2018) Repeat-associated non-AUG (RAN) translation and other molecular mechanisms in Fragile X tremor ataxia syndrome. *Brain Res* 1693: 43–54
29. Hagerman RJ, Berry-Kravis E, Hazlett HC, Bailey Jr DB, Moine H, Kooy RF, Tassone F, Gantois I, Sonenberg N, Mandel JL et al (2017) Fragile X syndrome. *Nat Rev Dis Primers* 3: 17065
30. Green KM, Glineburg MR, Kearse MG, Flores BN, Linsalata AE, Fedak SJ, Goldstrohm AC, Barmada SJ, Todd PK (2017) RAN translation at C9orf72-associated repeat expansions is selectively enhanced by the integrated stress response. *Nat Commun* 8: 2005
31. Kearse MG, Green KM, Krans A, Rodriguez CM, Linsalata AE, Goldstrohm AC, Todd PK (2016) CGG repeat-associated non-AUG translation utilizes a cap-dependent scanning mechanism of initiation to produce toxic proteins. *Mol Cell* 62: 314–322
32. Tabet R, Schaeffer L, Freyermuth F, Jambeau M, Workman M, Lee CZ, Lin CC, Jiang J, Jansen-West K, Abou-Hamdan H et al (2018) CUG initiation and frameshifting enable production of dipeptide repeat proteins from ALS/FTD C9ORF72 transcripts. *Nat Commun* 9: 152
33. Jackson RJ, Hellen CU, Pestova TV (2010) The mechanism of eukaryotic translation initiation and principles of its regulation. *Nat Rev Mol Cell Biol* 11: 113–127
34. Sonobe Y, Ghadge G, Masaki K, Sandoel A, Fuchs E, Roos RP (2018) Translation of dipeptide repeat proteins from the C9ORF72 expanded repeat is associated with cellular stress. *Neurobiol Dis* 116: 155–165
35. Kozak M (1986) Influences of mRNA secondary structure on initiation by eukaryotic ribosomes. *Proc Natl Acad Sci USA* 83: 2850–2854
36. Kozak M (1989) Circumstances and mechanisms of inhibition of translation by secondary structure in eucaryotic mRNAs. *Mol Cell Biol* 9: 5134–5142
37. Kozak M (1989) Context effects and inefficient initiation at non-AUG codons in eucaryotic cell-free translation systems. *Mol Cell Biol* 9: 5073–5080
38. Leppek K, Das R, Barna M (2018) Functional 5' UTR mRNA structures in eukaryotic translation regulation and how to find them. *Nat Rev Mol Cell Biol* 19: 158–174
39. Cheng W, Wang S, Mestre AA, Fu C, Makarem A, Xian F, Hayes LR, Lopez-Gonzalez R, Drenner K, Jiang J et al (2018) C9ORF72 GGGGCC repeat-associated non-AUG translation is upregulated by stress through eIF2alpha phosphorylation. *Nat Commun* 9: 51
40. Jan E, Thompson SR, Wilson JE, Pestova TV, Hellen CU, Sarnow P (2001) Initiator Met-tRNA-independent translation mediated by an internal ribosome entry site element in cricket paralysis virus-like insect viruses. *Cold Spring Harb Symp Quant Biol* 66: 285–292

41. Gao FB, Richter JD, Cleveland DW (2017) Rethinking unconventional translation in neurodegeneration. *Cell* 171: 994–1000
42. Green KM, Linsalata AE, Todd PK (2016) RAN translation—What makes it run? *Brain Res* 1647: 30–42
43. Fratta P, Mizielinska S, Nicoll AJ, Zloh M, Fisher EM, Parkinson G, Isaacs AM (2012) C9orf72 hexanucleotide repeat associated with amyotrophic lateral sclerosis and frontotemporal dementia forms RNA G-quadruplexes. *Sci Rep* 2: 1016
44. Sobczak K, Michlewski G, de Mezer M, Kierzek E, Krol J, Olejniczak M, Kierzek R, Krzyzosiak WJ (2010) Structural diversity of triplet repeat RNAs. *J Biol Chem* 285: 12755–12764
45. Zumwalt M, Ludwig A, Hagerman PJ, Dieckmann T (2007) Secondary structure and dynamics of the r(CG) repeat in the mRNA of the Fragile X mental retardation 1 (FMR1) gene. *RNA Biol* 4: 93–100
46. Chuang RY, Weaver PL, Liu Z, Chang TH (1997) Requirement of the DEAD-Box protein ded1p for messenger RNA translation. *Science* 275: 1468–1471
47. Hilliker A, Gao Z, Jankowsky E, Parker R (2011) The DEAD-box protein Ded1 modulates translation by the formation and resolution of an eIF4F-mRNA complex. *Mol Cell* 43: 962–972
48. Ihry RJ, Sapiro AL, Bashirullah A (2012) Translational control by the DEAD box RNA helicase belle regulates ecdysone-triggered transcriptional cascades. *PLoS Genet* 8: e1003085
49. Marsden S, Nardelli M, Linder P, McCarthy JE (2006) Unwinding single RNA molecules using helicases involved in eukaryotic translation initiation. *J Mol Biol* 361: 327–335
50. Sen ND, Zhou F, Harris MS, Ingolia NT, Hinnebusch AG (2016) eIF4B stimulates translation of long mRNAs with structured 5' UTRs and low closed-loop potential but weak dependence on eIF4G. *Proc Natl Acad Sci USA* 113: 10464–10472
51. Sen ND, Zhou F, Ingolia NT, Hinnebusch AG (2015) Genome-wide analysis of translational efficiency reveals distinct but overlapping functions of yeast DEAD-box RNA helicases Ded1 and eIF4A. *Genome Res* 25: 1196–1205
52. Soto-Rifo R, Rubilar PS, Limousin T, de Breyn S, Decimo D, Ohlmann T (2012) DEAD-box protein DDX3 associates with eIF4F to promote translation of selected mRNAs. *EMBO J* 31: 3745–3756
53. Rogers Jr GW, Richter NJ, Lima WF, Merrick WC (2001) Modulation of the helicase activity of eIF4A by eIF4B, eIF4H, and eIF4F. *J Biol Chem* 276: 30914–30922
54. Rogers Jr GW, Richter NJ, Merrick WC (1999) Biochemical and kinetic characterization of the RNA helicase activity of eukaryotic initiation factor 4A. *J Biol Chem* 274: 12236–12244
55. Svitkin YV, Pause A, Haghhighat A, Pyronnet S, Witherell G, Belsham GJ, Sonenberg N (2001) The requirement for eukaryotic initiation factor 4A (eIF4A) in translation is in direct proportion to the degree of mRNA 5' secondary structure. *RNA* 7: 382–394
56. Dhote V, Sweeney TR, Kim N, Hellen CU, Pestova TV (2012) Roles of individual domains in the function of DHX29, an essential factor required for translation of structured mammalian mRNAs. *Proc Natl Acad Sci USA* 109: E3150–E3159
57. Pisareva VP, Pisarev AV, Komar AA, Hellen CU, Pestova TV (2008) Translation initiation on mammalian mRNAs with structured 5'UTRs requires DExH-box protein DHX29. *Cell* 135: 1237–1250
58. Castilho-Valavicius B, Yoon H, Donahue TF (1990) Genetic characterization of the *Saccharomyces cerevisiae* translational initiation suppressors SUI1, SUI2 and SUI3 and their effects on HIS4 expression. *Genetics* 124: 483–495
59. Maag D, Algire MA, Lorsch JR (2006) Communication between eukaryotic translation initiation factors 5 and 1A within the ribosomal pre-initiation complex plays a role in start site selection. *J Mol Biol* 356: 724–737
60. Passmore LA, Schmeing TM, Maag D, Applefield DJ, Acker MG, Algire MA, Lorsch JR, Ramakrishnan V (2007) The eukaryotic translation initiation factors eIF1 and eIF1A induce an open conformation of the 40S ribosome. *Mol Cell* 26: 41–50
61. Pestova TV, Borukhov SI, Hellen CU (1998) Eukaryotic ribosomes require initiation factors 1 and 1A to locate initiation codons. *Nature* 394: 854–859
62. Pestova TV, Kolupaeva VG (2002) The roles of individual eukaryotic translation initiation factors in ribosomal scanning and initiation codon selection. *Genes Dev* 16: 2906–2922
63. Pisarev AV, Kolupaeva VG, Pisareva VP, Merrick WC, Hellen CU, Pestova TV (2006) Specific functional interactions of nucleotides at key –3 and +4 positions flanking the initiation codon with components of the mammalian 48S translation initiation complex. *Genes Dev* 20: 624–636
64. Singh CR, Curtis C, Yamamoto Y, Hall NS, Kruse DS, He H, Hannig EM, Asano K (2005) Eukaryotic translation initiation factor 5 is critical for integrity of the scanning preinitiation complex and accurate control of GCN4 translation. *Mol Cell Biol* 25: 5480–5491
65. Wek RC (2018) Role of eIF2alpha kinases in translational control and adaptation to cellular stress. *Cold Spring Harb Perspect Biol* 10: a032870
66. Jin P, Zarnescu DC, Zhang F, Pearson CE, Lucchesi JC, Moses K, Warren ST (2003) RNA-mediated neurodegeneration caused by the Fragile X premutation rCGG repeats in *Drosophila*. *Neuron* 39: 739–747
67. Krans A, Kearse MG, Todd PK (2016) Repeat-associated non-AUG translation from antisense CCG repeats in Fragile X tremor/ataxia syndrome. *Ann Neurol* 80: 871–881
68. Oh SY, He F, Krans A, Frazer M, Taylor JP, Paulson HL, Todd PK (2015) RAN translation at CGG repeats induces ubiquitin proteasome system impairment in models of fragile X-associated tremor ataxia syndrome. *Hum Mol Genet* 24: 4317–4326
69. Carvajal F, Vallejos M, Walters B, Contreras N, Hertz MI, Olivares E, Caceres CJ, Pino K, Letelier A, Thompson SR et al (2016) Structural domains within the HIV-1 mRNA and the ribosomal protein S25 influence cap-independent translation initiation. *FEBS J* 283: 2508–2527
70. Landry DM, Hertz MI, Thompson SR (2009) RPS25 is essential for translation initiation by the Dicistroviridae and hepatitis C viral IRESs. *Genes Dev* 23: 2753–2764
71. Hautbergue GM, Castelli LM, Ferraiuolo L, Sanchez-Martinez A, Cooper-Knock J, Higginbottom A, Lin YH, Bauer CS, Dodd JE, Myszczyńska MA et al (2017) SRSF1-dependent nuclear export inhibition of C9ORF72 repeat transcripts prevents neurodegeneration and associated motor deficits. *Nat Commun* 8: 16063
72. Castrillon DH, Gonczy P, Alexander S, Rawson R, Eberhart CG, Viswanathan S, DiNardo S, Wasserman SA (1993) Toward a molecular genetic analysis of spermatogenesis in *Drosophila melanogaster*: characterization of male-sterile mutants generated by single P element mutagenesis. *Genetics* 135: 489–505
73. Johnstone O, Deuring R, Bock R, Linder P, Fuller MT, Lasko P (2005) Belle is a *Drosophila* DEAD-box protein required for viability and in the germ line. *Dev Biol* 277: 92–101
74. Poulton JS, Huang YC, Smith L, Sun J, Leake N, Schleele J, Stevens LM, Deng WM (2011) The microRNA pathway regulates the temporal



- pattern of Notch signaling in *Drosophila* follicle cells. *Development* 138: 1737–1745
75. Spradling AC, Stern D, Beaton A, Rhem EJ, Laverty T, Mozden N, Misra S, Rubin GM (1999) The Berkeley *Drosophila* Genome Project gene disruption project: single P-element insertions mutating 25% of vital *Drosophila* genes. *Genetics* 153: 135–177
  76. Osterwalder T, Yoon KS, White BH, Keshishian H (2001) A conditional tissue-specific transgene expression system using inducible GAL4. *Proc Natl Acad Sci USA* 98: 12596–12601
  77. Guenther UP, Weinberg DE, Zubradt MM, Tedeschi FA, Stawicki BN, Zagore LL, Brar GA, Licatalosi DD, Bartel DP, Weissman JS et al (2018) The helicase Ded1p controls use of near-cognate translation initiation codons in 5' UTRs. *Nature* 559: 130–134
  78. Valentin-Vega YA, Wang YD, Parker M, Patmore DM, Kanagaraj A, Moore J, Rusch M, Finkelstein D, Ellison DW, Gilbertson RJ et al (2016) Cancer-associated DDX3X mutations drive stress granule assembly and impair global translation. *Sci Rep* 6: 25996
  79. Hinnebusch AG, Ivanov IP, Sonenberg N (2016) Translational control by 5'-untranslated regions of eukaryotic mRNAs. *Science* 352: 1413–1416
  80. Young SK, Wek RC (2016) Upstream open reading frames differentially regulate gene-specific translation in the integrated stress response. *J Biol Chem* 291: 16927–16935
  81. Kearse MG, Wilusz JE (2017) Non-AUG translation: a new start for protein synthesis in eukaryotes. *Genes Dev* 31: 1717–1731
  82. Chakrabarti A, Maitra U (1991) Function of eukaryotic initiation factor 5 in the formation of an 80 S ribosomal polypeptide chain initiation complex. *J Biol Chem* 266: 14039–14045
  83. Das S, Maiti T, Das K, Maitra U (1997) Specific interaction of eukaryotic translation initiation factor 5 (eIF5) with the beta-subunit of eIF2. *J Biol Chem* 272: 31712–31718
  84. Nanda JS, Saini AK, Munoz AM, Hinnebusch AG, Lorsch JR (2013) Coordinated movements of eukaryotic translation initiation factors eIF1, eIF1A, and eIF5 trigger phosphate release from eIF2 in response to start codon recognition by the ribosomal preinitiation complex. *J Biol Chem* 288: 5316–5329
  85. Nanda JS, Cheung YN, Takacs JE, Martin-Marcos P, Saini AK, Hinnebusch AG, Lorsch JR (2009) eIF1 controls multiple steps in start codon recognition during eukaryotic translation initiation. *J Mol Biol* 394: 268–285
  86. Saini AK, Nanda JS, Martin-Marcos P, Dong J, Zhang F, Bhardwaj M, Lorsch JR, Hinnebusch AG (2014) Eukaryotic translation initiation factor eIF5 promotes the accuracy of start codon recognition by regulating Pi release and conformational transitions of the preinitiation complex. *Nucleic Acids Res* 42: 9623–9640
  87. Pisareva VP, Pisarev AV (2014) eIF5 and eIF5B together stimulate 48S initiation complex formation during ribosomal scanning. *Nucleic Acids Res* 42: 12052–12069
  88. Loughran G, Sachs MS, Atkins JF, Ivanov IP (2012) Stringency of start codon selection modulates autoregulation of translation initiation factor eIF5. *Nucleic Acids Res* 40: 2898–2906
  89. Archbold HC, Jackson KL, Arora A, Weskamp K, Tank EM, Li X, Miguez R, Dayton RD, Tamir S, Klein RL et al (2018) TDP43 nuclear export and neurodegeneration in models of amyotrophic lateral sclerosis and frontotemporal dementia. *Sci Rep* 8: 4606
  90. Barmada SJ, Ju S, Arjun A, Batarse A, Archbold HC, Peisach D, Li X, Zhang Y, Tank EM, Qiu H et al (2015) Amelioration of toxicity in neuronal models of amyotrophic lateral sclerosis by hUPF1. *Proc Natl Acad Sci USA* 112: 7821–7826
  91. Malik AM, Miguez RA, Li X, Ho YS, Feldman EL, Barmada SJ (2018) Matr3-dependent neurotoxicity is modified by nucleic acid binding and nucleocytoplasmic localization. *Elife* 7: e35977
  92. Berthelot K, Muldoon M, Rajkowitsch L, Hughes J, McCarthy JE (2004) Dynamics and processivity of 40S ribosome scanning on mRNA in yeast. *Mol Microbiol* 51: 987–1001
  93. Lai MC, Chang WC, Shieh SY, Tarn WY (2010) DDX3 regulates cell growth through translational control of cyclin E1. *Mol Cell Biol* 30: 5444–5453
  94. Gruber AR, Lorenz R, Bernhart SH, Neubock R, Hofacker IL (2008) The Vienna RNA websuite. *Nucleic Acids Res* 36: W70–W74
  95. Lorenz R, Bernhart SH, Honer Zu Siederdisen C, Tafer H, Flamm C, Stadler PF, Hofacker IL (2011) ViennaRNA package 2.0. *Algorithms Mol Biol* 6: 26
  96. Zuker M (2003) Mfold web server for nucleic acid folding and hybridization prediction. *Nucleic Acids Res* 31: 3406–3415
  97. Grifo JA, Tahara SM, Leis JP, Morgan MA, Shatkin AJ, Merrick WC (1982) Characterization of eukaryotic initiation factor 4A, a protein involved in ATP-dependent binding of globin mRNA. *J Biol Chem* 257: 5246–5252
  98. Ray BK, Lawson TG, Kramer JC, Cladaras MH, Grifo JA, Abramson RD, Merrick WC, Thach RE (1985) ATP-dependent unwinding of messenger RNA structure by eukaryotic initiation factors. *J Biol Chem* 260: 7651–7658
  99. Hann SR (1994) Regulation and function of non-AUG-initiated proto-oncogenes. *Biochimie* 76: 880–886
  100. Ingolia NT, Brar GA, Stern-Ginossar N, Harris MS, Talhouarne GJ, Jackson SE, Wills MR, Weissman JS (2014) Ribosome profiling reveals pervasive translation outside of annotated protein-coding genes. *Cell Rep* 8: 1365–1379
  101. Meijer HA, Thomas AA (2002) Control of eukaryotic protein synthesis by upstream open reading frames in the 5'-untranslated region of an mRNA. *Biochem J* 367: 1–11
  102. Touriol C, Bornes S, Bonnal S, Audigier S, Prats H, Prats AC, Vagner S (2003) Generation of protein isoform diversity by alternative initiation of translation at non-AUG codons. *Biol Cell* 95: 169–178
  103. Ivanov IP, Loughran G, Sachs MS, Atkins JF (2010) Initiation context modulates autoregulation of eukaryotic translation initiation factor 1 (eIF1). *Proc Natl Acad Sci USA* 107: 18056–18060
  104. Kozel C, Thompson B, Hustak S, Moore C, Nakashima A, Singh CR, Reid M, Cox C, Papadopoulos E, Luna RE et al (2016) Overexpression of eIF5 or its protein mimic 5MP perturbs eIF2 function and induces ATF4 translation through delayed re-initiation. *Nucleic Acids Res* 44: 8704–8713
  105. Tang L, Morris J, Wan J, Moore C, Fujita Y, Gillaspie S, Aube E, Nanda J, Marques M, Jangal M et al (2017) Competition between translation initiation factor eIF5 and its mimic protein 5MP determines non-AUG initiation rate genome-wide. *Nucleic Acids Res* 45: 11941–11953
  106. Bol GM, Raman V, van der Groep P, Vermeulen JF, Patel AH, van der Wall E, van Diest PJ (2013) Expression of the RNA helicase DDX3 and the hypoxia response in breast cancer. *PLoS One* 8: e63548
  107. Brai A, Fazi R, Tintori C, Zamperini C, Bugli F, Sanguinetti M, Stigliano E, Este J, Badia R, Franco S et al (2016) Human DDX3 protein is a valuable target to develop broad spectrum antiviral agents. *Proc Natl Acad Sci USA* 113: 5388–5393
  108. Samal SK, Routray S, Veeramachaneni GK, Dash R, Botlagunta M (2015) Ketorolac salt is a newly discovered DDX3 inhibitor to treat oral cancer. *Sci Rep* 5: 9982
  109. Pandey UB, Nie Z, Batlevi Y, McCray BA, Ritson GP, Nedelsky NB, Schwartz SL, DiProspero NA, Knight MA, Schuldiner O et al (2007)

- HDAC6 rescues neurodegeneration and provides an essential link between autophagy and the UPS. *Nature* 447: 859–863
110. Hafner M, Landthaler M, Burger L, Khorshid M, Hausser J, Berninger P, Rothballer A, Ascano Jr M, Jungkamp AC, Munschauer M *et al* (2010) Transcriptome-wide identification of RNA-binding protein and microRNA target sites by PAR-CLIP. *Cell* 141: 129–141
  111. Rakotondrafara AM, Hentze MW (2011) An efficient factor-depleted mammalian *in vitro* translation system. *Nat Protoc* 6: 563–571
  112. Caschera F, Noireaux V (2015) Preparation of amino acid mixtures for cell-free expression systems. *Biotechniques* 58: 40–43
  113. Simsek D, Tiu GC, Flynn RA, Byeon GW, Leppke K, Xu AF, Chang HY, Barna M (2017) The mammalian ribo-interactome reveals ribosome functional diversity and heterogeneity. *Cell* 169: 1051–1065 e1018
  114. Saudou F, Finkbeiner S, Devys D, Greenberg ME (1998) Huntingtin acts in the nucleus to induce apoptosis but death does not correlate with the formation of intranuclear inclusions. *Cell* 95: 55–66
  115. Barmada SJ, Skibinski G, Korb E, Rao EJ, Wu JY, Finkbeiner S (2010) Cytoplasmic mislocalization of TDP-43 is toxic to neurons and enhanced by a mutation associated with familial amyotrophic lateral sclerosis. *J Neurosci* 30: 639–649